

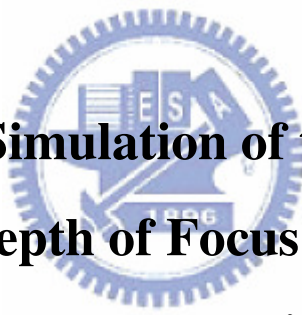
國立交通大學

電子工程學系

電子研究所碩士班

碩士論文

使用一次曝光和二元光罩來產生擁有良好聚焦
深度的細線之模擬與研究



**The Study and Simulation of the Line Pattern
having large Depth of Focus by using only
Single Exposure and Binary Mask**

研究生：曹人傑

Jen-Chieh Tsao

指導教授：羅正忠 博士

Dr. Jen-Chung Lou

邱碧秀 博士

Dr. Bi-shiou Chiou

中華民國九十六年七月

使用一次曝光和二元光罩來產生擁有良好聚焦

深度的細線之模擬與研究

The Study and Simulation of the Line Pattern

having large Depth of Focus by using only

Single Exposure and Binary Mask

研究生：曹人傑

Student：Jen-Chieh Tsao

指導教授：羅正忠博士

Advistor：Dr. Jen-Chung Lou

邱碧秀 博士

Dr. Bi-shiou Chiou

國立交通大學

電子工程學系

電子研究所碩士班

碩士論文

A Thesis

Submitted to Institute of Electronics

College of Electrical and Computer Engineering

National Chiao Tung University

in Partial Fulfillment of the Requirements

for the Degree of Master of Science

in Electronic Engineering

July 2007

Hsinchu, Taiwan, Republic of China

中華民國九十六年七月

使用一次曝光和二元光罩來產生擁有良好聚焦

深度的細線之模擬與研究

研究生：曹人傑

指導教授：邱碧秀 博士

羅正忠 博士

國立交通大學

電子工程學系



電子研究所碩士班

摘要

我們發現當一條暗線獨自被曝光時會有較差的結果，可是當這條暗線是被兩條細的亮線所包圍時，經由適當的曝光條件，我們能夠得到一條極佳的暗線，而這條暗線的寬度能小於100nm，此外，藉由這個曝光方式，我們只需要使用二元光罩即可得到擁有如此良好寬度的暗線。

不過使用上述的方式所得到的暗線，在相鄰的兩條細暗線間，會得到一條不

想得到的粗暗線，因此，我們必須另外增加一道曝光過程將此不希望出現的粗暗線給清除掉，所以總共需要兩次曝光，而為了能夠減少曝光的次數，我們將原本會產生粗暗線的部份改成部分透光但像位不變的光罩，而藉由這樣的改變我們能提升此處的光強，所以使得原本不曝光的部分變成曝光，因此只需一次曝光即可得到想要的細線。

最後，我們使用一群適當週期排列的細線，此細線的寬度小於曝光的極限因而不會被顯現出來，接著再適度調整週期，藉由暗線和亮線所佔面積的不同來得到想要的穿透量，再將這群週期排列的暗線取代先前所提不曝光的區域，藉此得到只需使用一次曝光和二元光罩即可得到良好細線的方法。



The Study and Simulation of the Line Pattern having large Depth of Focus by using only Single Exposure and Binary Mask

Student: Jen-Chieh Tsao

Advisors: Dr. Bi-shiou Chiou

Dr. Jen-Chung Lou

Department of Electronics Engineering & Institute of Electronics

National Chiao Tung University, Hsinchu, Taiwan



Abstract

It is discovered by optical image calculations that a dark mask line between two bright mask lines can be imaged with very fine width under a modified illumination. The fine dark line pattern with the width finer than 100 nm is formed by the application of the image generated by this method. And with this method you can just use only the binary mask to get the fine line pattern, but there will be opaque regions between the pair of bright lines. So it needs another exposure mask to erase the unwanted region. In order to prevent adding another exposure step, we replace the

opaque regions to be the attenuating non-phase-shifting (Atten-NPS) mask. When the corrected mask is illuminated by an obliquely incident light with a specific incident angle, very sharp dark line image is formed at center of the bright lines. Because the outside of the pair is Atten-NPS area, image intensity for this area can become much higher than a slice level of the central dark line image, resulting in no resist pattern at the outside of the pair. So we need just only a single exposure step and can get the wanted line pattern. Finally, we change the Atten-NPS region to be the thin dark lines which is so small so will not to be printed. In the last method, we can have the advantages of former two methods that using only the binary mask and single exposure to get the fine line patterns.



致謝

轉眼間，兩年的碩士學業很快就要劃下句號了。

首先我想感謝我的指導教授羅正忠博士和邱碧秀博士，在繁忙的工作之餘依然耐心地給予實驗室學生們學術上的指導與勉勵，由於您的細心指導與教誨，讓我在研究上與許多做人處事上都有莫大的收穫，真的使我受益匪淺，在這裡對老師致上我內心最高的謝意，感謝您兩年來的教導。

此外，我還要感謝張仲興與胡國信學長的指導以及您所留下來的寶貴資源讓我在研究上得以順利解決許多難題及模擬實驗，謹此致上最誠摯的謝意。同時也要感謝曾經一起同甘苦同學們：建彰、忠樂、彥銘、德安、智仁、睿龍、宏仁、俐婷、大峰、信智、勝凱，謝謝你們在生活及精神上給予的支持。

最後我要感謝我的家人，感謝我的父母多年來的苦心的栽培與一再的鼓勵，給予我正確的人生觀以及待人接物的道理，讓我有信心以及勇氣克服一切，此外還要感謝你們無怨無悔的付出讓我無後顧之憂地完成我的碩士學業，我的生命，是你們的恩賜；我今日的成就，你們是幕後的推手，謝謝你們。在此獻上我內心最深的感恩，辛苦你們了：爸、媽。

Contents

Abstract (Chinese).....	i
Abstract (English).....	iii
Acknowledgements.....	v
Contents.....	vi
List of Figures.....	viii

Chapter 1 Introduction

1-1 Background.....	1
1-2 Resolution Enhancement Techniques.....	2
1-2.1 Off-Axis Illumination.....	3
1-2.2 Phase Shift Mask.....	4
1-2.3 Two versus three beam imaging.....	6
1-3 Motivation.....	6
1-4 Organization of This Thesis.....	7

Chapter 2 Image Formation and Quality Parameter

2-1 Image formation in projection optics.....	14
2-2 Contrast.....	15
2-3 Normalized Image Log Slop.....	16
2-4 Mask Error Enhancement Factor.....	16
2-5 Process Window.....	16

Chapter 3 Principle of Iso-Focal

3-1 Link between the iso-focal point and the DOF.....	21
3-1.1 Definition of the iso-focal point.....	21
3-1.2 Influence of the iso-focal position on the DOF.....	21
3-2 Evolution of the iso-focal point.....	22
3-2.1 Theoretical background.....	22
3-2.2 Binary and attenuated masks.....	23
3-2.3 Alternated PSM masks.....	25
3-3 Analysis of the iso-focal variation.....	26
3-4 Improvement of the DOF.....	27

Chapter 4 Principle and Simulation

4-1 The use of pair of bright lines.....	33
4-1.1 Concept of pair of bright lines.....	33
4-1.2 The effect of the width of the bright lines on the image.....	34
4-1.3 The effect of the width of the dark line on the image.....	34
4-1.4 Image formation with Att-PSM.....	35
4-2 Change the dark line between the pair lines with Atten-NPS.....	35
4-2.1 Concept of the use of Atten-NPS.....	35
4-2.2 Simulation of the advanced one with binary mask.....	36
4-2.3 Compare of the use of 6% and 20% Atten-NPS.....	36
4-3 Change the Atten-NPS with binary mask.....	37

Chapter 5 Conclusion

5-1 Conclusion.....	51
---------------------	----

Reference	54
------------------------	----



List of Figures

Fig 1-1 Lithography requirement and development trend of lithographic technologies.

Fig 1-2 the schematic design of a typical optical exposure tool

Fig 1-3 schematic structure of exposure and resolution enhancement technologies

Fig 1-4 Illumination beams, phase and amplitude of electric field, d spatial frequency vectors

Fig 1-5 Filling of the projection pupil for (a) annular and (b) quadrupole

Fig 1-6 binary (Left) and Alternating Phase Shifting (Right)

Fig 1-7 Attenuated Phase Shifting

Fig 1-8 Subresolution-Assisted Phase Shifting

Fig 1-9 Rim Phase Shifting

Fig. 1-10 edge PSM

Fig 1-11 sub resolution Utt PSM

Fig 1-12 Two versus three beam imaging

Fig 2-1 Schematic view of a generic projection system and principle of image formation

Fig 2-2 contrast

Fig 2-3 Normalized Image Log Slope

Fig 2-4 The effect of focus and exposure on the resulting resist profile: (a) linewidth, (b) sidewall angle, and (c) resist loss.

Fig. 2-5 contours of constant CD versus focus and exposure

Fig 2-6 The focus-exposure process window constructed from contours of the specifications for linewidth, sidewall angle and resist loss. Shaded area the shows overall process window.

Fig 2-7 The process window (a) is analyzed by fitting all of the maximum rectangles, then plotting their height (exposure latitude) versus their width (depth of focus) as in (b)

Fig.3-1 Position of the iso-focal point in the aerial image curves. $CD(\text{mask})=0.12\mu\text{m}$; $p=0.30\mu\text{m}$, $\lambda=193\text{nm}$, $NA=0.63$ and $\sigma=0.5/0.8$ (annular illumination)

Fig 3-2 Position of the iso-focal point compared to the target CD and the corresponding DOF as function of the pitch. $CD(\text{mask})=0.15\mu\text{m}$; $p=0.30\mu\text{m}$, $\lambda=193\text{nm}$, $NA=0.63$ and $\sigma=0.5/0.8$ (annular illumination)

Fig 3-3 Schematic sketch of a lithographic system

Fig 3-4 Diffracted waves captured by the pupil plane

Fig. 3-5 Binary mask or attenuated phase shift mask imaging for periodic line patterns:

(a) schematic structure of exposure optics, (b) transmitted amplitude of light at mask, (c) diffracted waves for partially coherent light.

Fig 3-6 Diffracted waves of periodic line patterns for partially coherent light when (a)

all components (-1st, 0th, and +1st) are transmitted, (b) either the -1st or +1st component is eliminated for some point sources, (c) both the -1st and +1st components are eliminated for some point sources, (d) some pairs of -1st and 0th components, or of 0th and +1st components are transmitted, (e) both the -1st and +1st components are completely eliminated. The areas denoted as S_3 , S_2 , and S_1 correspond to the source area for three-beam interference, two-beam interference, and only 0th order wave transmission.

Fig. 3-7 Phase-shift mask imaging for periodic line patterns: (a) schematic structure of

exposure optics, (b) transmitted amplitude of light at mask, (c) diffracted waves for partially coherent light

Fig. 3-8 The theoretical evolution of the iso-focal intensity threshold of a 150nm line

with a conventional illumination ($\lambda=193\text{nm}$, $\text{NA}=0,63$ and $\sigma=0,8$) as function of the pitch for three type of masks: binary, 10% attenuated PSM and alternated PSM

Figure 3-9 Evolution of I_β et I_{S_2} for a 150nm (binary mask) with a conventional

illumination ($\lambda=193\text{nm}$, $\text{NA}=0.63$ and $\sigma=0.80$). S_2 is the normalized area of the two orders interference

Fig. 3-10 Evolution of the iso-focal threshold of a 150nm line as function of the pitch

with the simple exposure, SRAF (sub resolution assist features) and the CODE techniques using a conventional illumination ($\lambda=193\text{nm}$, $\text{NA}=0,63$ and $\sigma=0,8$).

Fig. 4-1 original mask for the formation of dark lines

Fig. 4-2 Schematic mask pattern for this pattern formation method. Upper shows for fine dark line image formation and lower shows a mask for 2 nd exposure to erase undesirable dark line pattern between the pairs of bright lines.

4-1 original mask for the formation of dark lines

Fig. 4-3 Image intensity profiles of a bright lines pair mask pattern. CoG mask,

$\text{NA}=0.65$ Fig. 4-4 The same image intensity profile as in Fig. 5 in large scale to appear the effective image contrast with focus offset

Fig. 4-5 Image intensity profiles of a bright lines pair mask under conditions of CoG mask and conventional illumination. $NA=0.60$, $\sigma=0.85$

Fig. 4-6 Image intensity profiles with changing bright line width of the bright lines pair for the width of (a)190nm (b) 170nm (c) 150nm

Fig. 4-7 Image intensity profiles with changing dark line width between the bright lines pair (a) 190nm (b) 170nm (c) 150nm

Fig. 4-8 Image intensity profiles and process window for (a) with binary mask (b) with 6% atten-PSM

Fig. 4-9 Typical mask patterns and images formed by the mask patterns. (upper) and (lower) show those of the former work and the advanced one, respectively

Fig. 4-10 mask of isolated line with changing the transmission of Atten-NPS area

Fig 4-11 aerial image for (a) atten-NPS=20% (b) atten-NPS=25% (c) atten-NPS=30% (dark line=170nm, bright line=90nm, pitch=0.77)

Fig 4-12 process window for (a) atten-NPS=20% (b) atten-NPS=25% (c) atten-NPS=30% (dark line=170nm, bright line=90nm, pitch=0.77)

Fig 4-15 aerial image for (a) atten-PSM=6%, atten-NPS=20% (b) atten-PSM=6%, atten-NPS=25% (c) atten-PSM=6%, atten-NPS=30% (d) atten-PSM=20%, atten-NPS=20% (e) atten-PSM=20%, atten-NPS=25% (f) atten-PSM=20%, atten-NPS=30% (dark line=170nm, bright line=90nm, pitch=0.77)

Fig 4-16 process window for (a) atten-PSM=6%, atten-NPS=20% (b) atten-PSM=6%, atten-NPS=25% (c) atten-PSM=6%, atten-NPS=30% (d) atten-PSM=20%, atten-NPS=20% (e) atten-PSM=20%, atten-NPS=25% (f) atten-PSM=20%, atten-NPS=30% (dark line=170nm, bright line=90nm, pitch=0.77)

Fig.4-17 (a) mask (b) aerial image of Atten-NPS=0.25 (width=420nm) (c) aerial image of 0.07/0.07/0.07/0.07/0.07

Fig 4-18 aerial image for (a) Atten-NPS =25% (b) equal binary mask (dark line=170nm, bright line=nm, pitch=0.)

Fig 4-19 process window for (a) Atten-NPS =25% (b) equal binary mask (dark line=170nm, bright line=nm, pitch=0.)

Fig 5-1 scheme of the three methods

Fig 5-2 process window and aerial image for three methods

Chapter 1

Introduction

1-1 Background

Lithography has been one of the key drivers for the semiconductor industry. Moore's Law states that the number of devices on a chip doubles every 18 months. There are three main constituents of the technology improvements that have kept the industry on this pace for more than 30 years. They are lithography, increased wafer size, and design. Roughly half of the density improvements have been derived from improvements in lithography. With the cost to fabricate a wafer remaining roughly constant, independent of size or content, this has resulted in a 30% reduction in cost per function per year over this period [1].

The trend of minimum feature sizes of ultra large-scale integrated (ULSI) devices and lithographic performances is shown in Fig. 1-1. The integration level has increased fourfold every two or three year. Because advances in optics and resist materials, optical lithography is still the most important lithographic technologies in the industrial environment. However, the minimum feature size of ULSI devices becomes smaller than wavelength of exposure light used in the optical system. In fact, 64M bit DRAMS have been developed with a minimum feature size of 0.19 μ m which is smaller than exposure wavelength of KrF excimer laser light (0.248 μ m). Ways to obtain high resolution and better alignment accuracy with minimal increase in cost and minimal reduction in throughput are needed. Besides the resolution enhanced optical lithography technique, electron beam (EB) lithography and the combination of EB and optical technologies have a chance to play important roles in the mass-production of ULSI devices. X-ray lithography is also an option because they are considered an extension of present optical lithography using extremely short wavelength. These technologies have not been used much in industry, though, because their throughput is lower than optical technique and equipment cost is high.

The schematic design of a typical optical exposure tool is shown in Fig. 1-2. The

tool consists of a light source, a condenser, a stage for mask at the object plane, a projection lens with very small wavefront aberration, and a stage for the wafer. At each point on the wafer, light converges with a cone of half angle of θ . The numerical aperture of the projection lens is defined as $NA = \sin\theta$. The resolution of a lithography system is usually expressed in terms of its wavelength and numerical aperture (NA) as

$$\text{Resolution} = k_1 \frac{\lambda}{NA} \quad (1-1)$$

where the constant k_1 is dependent on the process being used. In IC manufacturing, typical values of k_1 range from 0.5 to 0.8, with a higher number reflecting a less stringent process.

The NA of optical lithography tools ranges from about 0.5 to 0.6 today.

Increased NA is, of course, another route to improved resolution in optical lithography. Improved optical designs aided by sophisticated computer modeling are enabling larger NA lenses to be designed. KrF systems with NA will be available shortly with NA systems being designed. The penalties for these very high-NA systems are primarily in cost and depth of focus (DOF). The cost of the lens and, thus, the lithography system and wafers printed by it scales roughly with the cube of the NA (volume of lens material). At these large NAs, the weight and size of the lenses also presents many practical issues. The DOF of a system can also be characterized by the wavelength and NA as

$$DOF = k_2 \frac{\lambda}{NA^2} \quad (1-2)$$

Where k_2 is also a process-dependent parameter generally taken to have the same value as k_1 . This clearly shows the penalty in DOF for high-NA systems. Reduced DOF requires extremely tight control and planarity in the wafer process. For even a modest (0.6) NA system, the DOF is only a few hundred nanometers. Usable NA will be limited to something less than the theoretical limit of NA by DOF considerations as well as effects caused by refraction of the high angle light and polarization effects in the resist film. A practical maximum is currently thought to be NA.

1-2 Resolution Enhancement Techniques

The concepts of increasing resolution of optical lithography are summarized in Fig 1-3. In the exposure tool, the mask is illuminated by light from the light source, and patterns on the mask are projected onto the wafer surface through the projection

exposure lens. Resolution enhancement is achieved by modifying the source shape, by using special mask that introduce a phase difference, or by placing a filter [3-5] at the pupil plane of exposure lens. Other methods such as multi-exposure method to align multi-focal level [6-8], and surface imaging process for low optical constant condition have been proposed. In the following, we will introduce some often used Resolution Enhancement Techniques.

1-2.1 Off-Axis Illumination

Off-axis illumination [9-13] takes advantage of spatial frequency shifting of a given object. It can best be illustrated with a simple grating object. The grating being periodical, contains discrete spatial frequency components, namely, the 0th, ± 1 st, ± 2 nd, ... orders. When the minimum feature is of interest, only the first order frequencies are preserved so that the resolution potential of the imaging lens can be fully utilized. This situation is shown in Fig. 1-4a where on-axis illumination is chosen. The spatial frequency spectrum consists of the vertically oriented 0th order beam and the ± 1 st order beams whose angle is a function of the periodicity of the grating. A smaller periodicity produces large spatial frequencies, thus larger diffraction angles in the ± 1 st order beams. When the feature size is too small, i.e. the spatial frequency too high, the angle of the diffracted beams becomes larger than the acceptance angle of the imaging lens and the ± 1 st order beams are rejected. Only the 0th order beam passes. The image becomes a structureless uniform beam.

The electric field on a binary intensity mask (BIM) is simply 1 and 0 at the transparent and opaque parts of the mask, respectively. The actual field is obviously much more complicated when exact electromagnetic diffraction is taken into account. Here, for illustration purposes, the simple assumption works best. The intensity at the mask plane is proportional to the square of the simplified electric field and is shown to be 1 and 0, following the electric field completely. The intensity at the image plane is uniform just as if no object is present, because the ± 1 st order beams are not accepted by the lens. Only the 0th order beam, which has no information content, passes through the lens. The intensity of the image is reduced because the energy of the rejected beams are not recovered.

Figure 1-4b shows the situation of a single collimated illumination beam obliquely incident on the mask, thus off-axis. The three beams shown in Fig. 1-4a are now tilted by the incident angle of the illumination. When the angle is adjusted to make the 0th order and one of the 1st order beams symmetrical with respect to the

optical axis, the largest angular spread between the two beams is possible without being cutoff by the acceptance angle of the lens, thus the highest resolution is achieved. However, the other 1st order beam is cutoff, resulting in a lower exposing intensity.

In Fig. 1-4c, two symmetrically opposed beams are used. When the angle of the illumination is optimized for a given periodic object, the 0th order of the left beam coincides with the 1st order of the right beam and the 0th order of the right beam coincides with the -1st order of the left beam as shown in the figure. The image consists of a single frequency component and is well reproduced.

When objects of a lower spatial frequency in Fig. 1-4d are illuminated by the same set of beams, the spatial frequency vectors no longer coincide, producing additional spatial frequencies. These frequencies can induce a worse imaging characteristic than that from on-axis illumination.

Off-axis illumination contains a lot of kinds, and the most kinds are annular and quadrupole. The two kinds of OAI are shown in Fig.1-5. In Figure 1-5a, the filling of the projection pupil in DUV lithography (NA=0.6) using annular illumination ($\sigma_{\text{outer}}=0.8/\sigma_{\text{inner}}=0.5$) is shown for 180nm dense lines. The zero order diffraction signal is fully captured. This mode does not contain any information about the reticle periodicity. In the case of a binary reticle containing a line/space pattern, the power carried by the zero order is just the average transmitted intensity level and is often referred to as the DC-component. The aerial image is formed by two-beam interference of the zero order and one of the first order beams. However, both first order diffraction modes which carry the modulation information from the reticle, partially lie outside the entrance pupil. In this way, a significant part of the modulation signal is lost when using annular illumination. By using quadrupole illumination (round poles with ($\sigma_{\text{outer}}=0.8$ and $\sigma_{\text{inner}}=0.5$), the amount of first order signal captured by the lens increases as depicted in Figure 1-5b. In this way, quadrupole illumination enhances the ratio of first to zero order. It can be easily demonstrated that the higher the ratio of first to zero order, the higher the contrast of the aerial image. Therefore, the exposure latitude should be higher in the case of quadrupole illumination.

1-2.2 Phase Shift Mask

The phase shifting mask (PSM) technique [14-18], as well as illumination optimization, can improve the contrast of the optical image to improve the resolution

and DOF. The potential improvement is a reduction of K_1 by between 0.15 and 0.3, with a tolerable reduction in K_2 . That is, the DOF can be maintained at a fixed value but the resolution is improved. In follows, we will introduce some kinds of PSM.

(a) Alternating Phase Shifting [19]

This system is characterized by phase shifting every other element in a closely packed array. The Alt PSM approach is shown in Fig 1-6(Right). In comparison to the binary intensity mask (BIM) in Fig. 1-6(Left). In the Alt PSM, the electric field amplitude is -1 at the shifted areas on the mask. This -1 amplitude effectively reduces the spatial frequency of the electric field so that it is less inhibited by the lens transfer function and forms a higher-contrast amplitude image at the wafer plane. When this electric field is recorded by the photoresist, only the intensity which is proportional to the square of the electric field amplitude can be recorded. Hence the reduced spatial frequency is doubled back to the original frequency but the image has much more contrast. Edge contrast is also improved because the electric field must pass through a zero to -1 amplitude, which assures a zero intensity at the wafer.

(b) Attenuated Phase Shifting[20]

The Att PSM is another PSM approach that applies to arbitrary mask layouts. It can be implemented on either a transmissive mask or a reflective one. The dark areas of the mask can be phase shifted to Π , but with an attenuated amplitude to prevent producing too much light in these areas (Fig 1-7). The negative amplitude provides the desired improvement in image edge contrast, and the attenuation prevents the negative amplitude from becoming too large and subsequently exposing the resist.

(c) Subresolution-Assisted Phase Shifting[21]

The Alternating PSM method demonstrates the potential of phase shifting. However, it requires closely packed patterns to be effective. In actual circuit layouts there are many situations where critical dimensions are sufficiently far away from any adjacent patterns to provide phase shifting. In order to provide phase shifting for isolated openings such as contact holes and line openings, subresolution phase shifters are introduced (Fig 1-8).

The dimension of these phase shifters is below the resolution limit of the optical imaging system. Thus, images cannot be printed. Their sole function is to enhance the edge contrast of the pattern of interest.

(d) Rim Phase Shifting

Subresolution-Assisted PSM and Alternating PSM are still limited by the

inability to provide phase shift to opaque patterns. Rim PSM (Fig 1-9) overcomes such a problem and can be applied to an arbitrary mask layout. Here, phase shifting only takes place at the rim of the mask patterns. The center of the patterns is blocked by the absorber to prevent large areas of negative amplitude from producing bright areas where they are supposed to be dark. Again bright areas result from negative or positive field amplitudes because the photoresist can only detect intensity which is proportional to the square of the electric field. Note that edge contrast enhancement is now the sole imaging improving function of these phase shifters.

(e) Unattenuated Phase Shifting [22-24]

Transparent phase shifters can also be used to improve the optical image without having to use a mask absorber. The transparent characteristics can be taken advantage of in spatial frequency doubling, or to make an opaque line image from the phase shifted edge (edge PSM) as shown in Fig 1-10, respectively. Small phase shifter patterns in Utt PSM become opaque patterns because the opaque edges of these patterns are not resolvable from each other. Hence, as shown in Fig 1-11, small opaque features can be formed by this sub resolution Utt Psm (SU PSM) and large opaque areas can be synthesized with many SU features.

1-2.3 Two versus three beam imaging

The light then passes through the reticle, where it is diffracted into orders. The orders are collected by the entrance pupil of the lens and recombined at the focal plane to create an image on the wafer. At the resolution limit of the lens (Figure 1-12) the entrance pupil only captures the zero and first orders of the diffracted light.

Changing the illuminator setup can have a marked effect on image contrast; this is especially true when comparing conventional ($\theta=0$) to off-axis illumination ($\theta>0$). The reason can be explained by comparing the way in which the first and second orders interfere (Figure 1-12). Conventional illumination results in a three beam interference effect, while only two beams interfere in the off-axis case.

1-3 Motivation

In recent days, gate length in advanced CMOS logic devices has become much shorter than an exposure wavelength in applied optical lithography. Then, RETs such as sub-resolution assist feature (SRAF) , double exposure by alternating phase shift mask (Alt-PSM) with trim mask and Cr-less phase shift lithography (CPL) are needed

to form a resist pattern of these devices. While SARF exposure utilize a single layer mask and single exposure, the performance of this RET is not so great. On the other hand, so called strong RETs, such as Alt-PSM or CPL show excellent lithography performance. But, these methods require phase shift mask with complicated structure and/or double exposure to form one layer pattern, resulting in higher cost and longer turn around time. In 2001, some of authors have proposed a novel RET which utilize simple binary masks [27]. In the technique, a pair of bright lines in dark field of binary mask or Atten-PSM is applied to form fine dark line image. With a specific modified illumination, ~60 nm isolated space pattern formation has been achieved with negative-tone chemically amplified resist. But this method still needs two times exposure, so we hope to find another method to resolve this problem.

1-4 Organization of This Thesis

This thesis includes five chapters. In chapter 1, we make an introduction to describe the background of the optical lithography and the role in the semiconductor industry that optical lithography is playing. In addition, we make a brief to describe simple concept of the optical lithography. Then, we describe the motivation of this thesis. Finally, we introduce four kinds of the well-known RETs. They are OAI, PSM, FLEX and lens pupil-filtering respectively.

In chapter 2 , we will first specify our simulation model and condition. Then, we will illustrate and define the parameters of image quality with mathematical formula or example.

In chapter 3, we will explain the principle of iso-focal. Then, we also will discuss the effect of the iso-focal to the depth of focus, and introduce how to decrease the iso-focal intensity threshold.

In chapter 4, we first introduce the way to use only binary mask to gain the fine line pattern. Then, we will replace some regions of above method to gain a similar mask, and when using the mask we need only one time of exposure to gain the similar result as former. Finally, we will use another method which can have the advantages needing only binary mask and one time exposure of above two.

In chapter 5 , we will make a conclusion of this thesis.

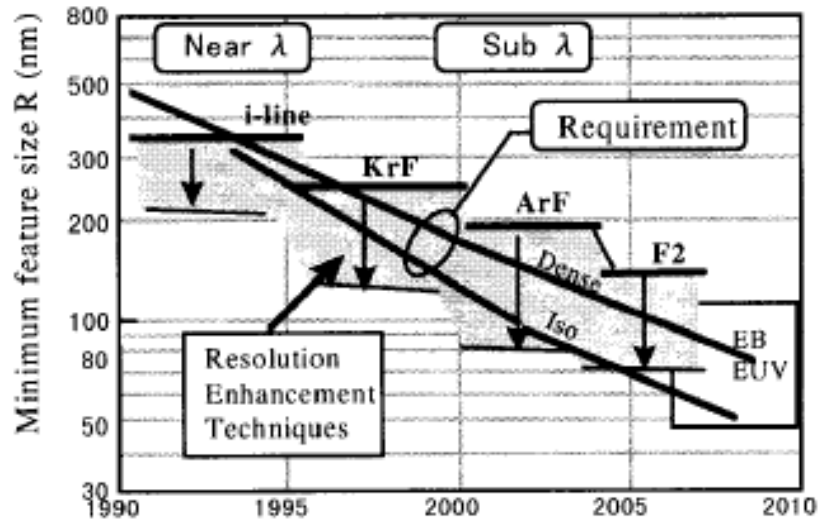


Fig 1-1 Lithography requirement and development trend of lithographic technologies.[2]

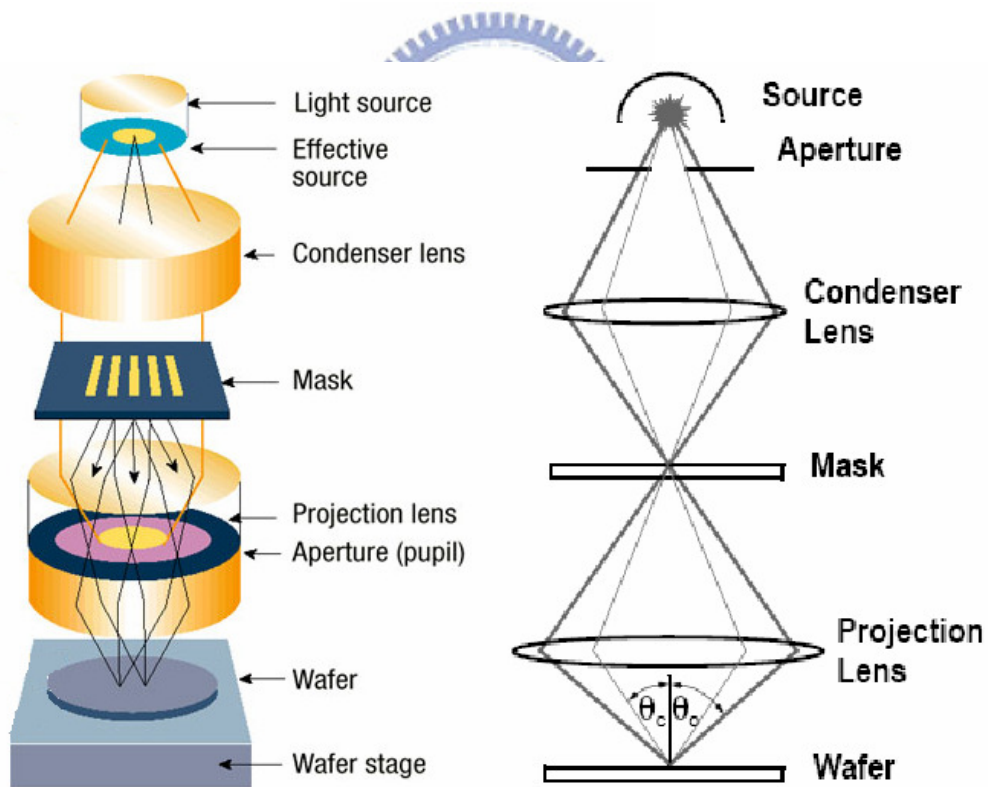


Fig 1-2 the schematic design of a typical optical exposure tool [2]

Resolution enhancement technologies

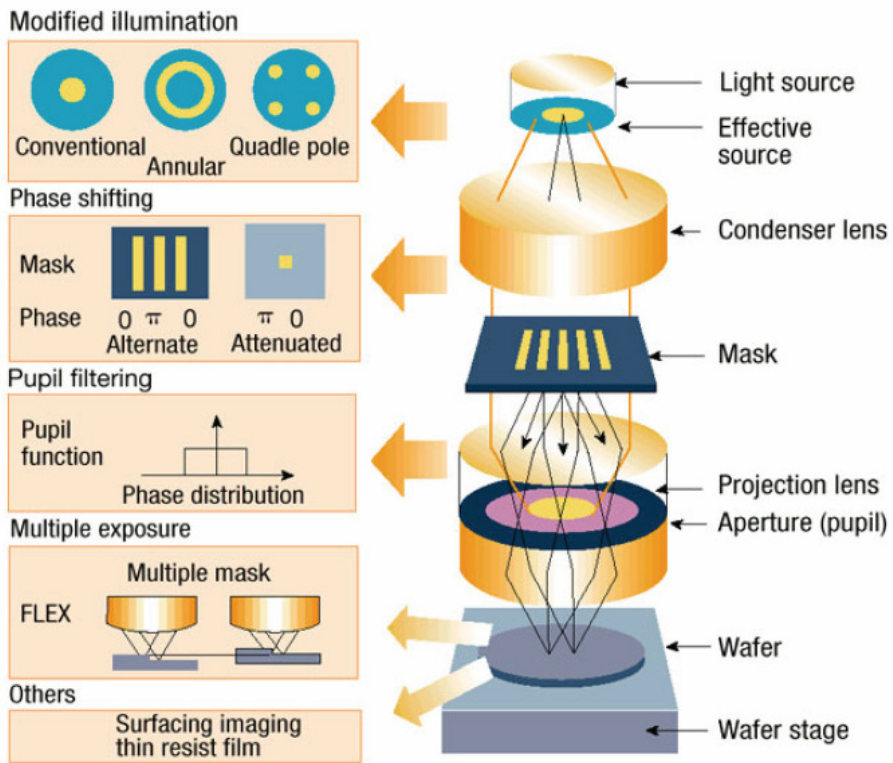


Fig 1-3 schematic structure of exposure and resolution enhancement technologies [2]

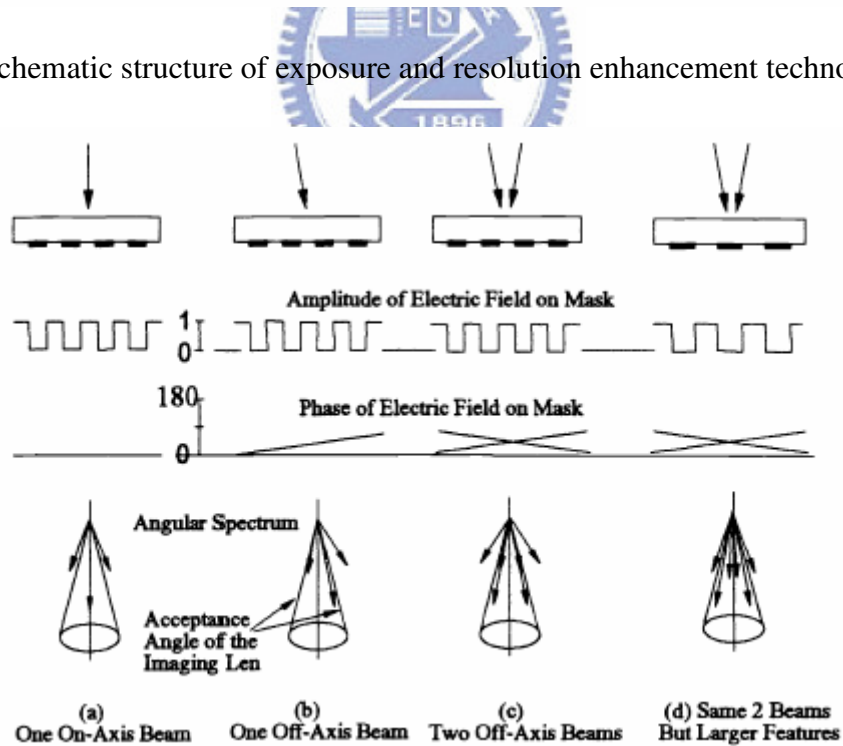
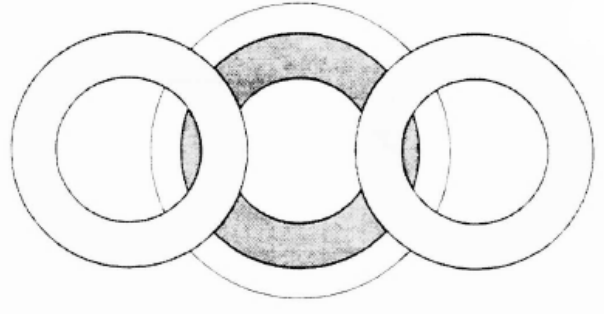
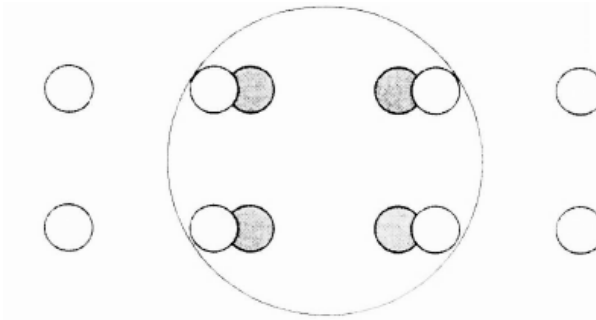


Fig 1-4 Illumination beams, phase and amplitude of electric field, d spatial frequency vectors [13]



(a) Annular



(b) Quadrupole

Fig 1-5 Filling of the projection pupil for (a) annular and (b) quadrupole [25]

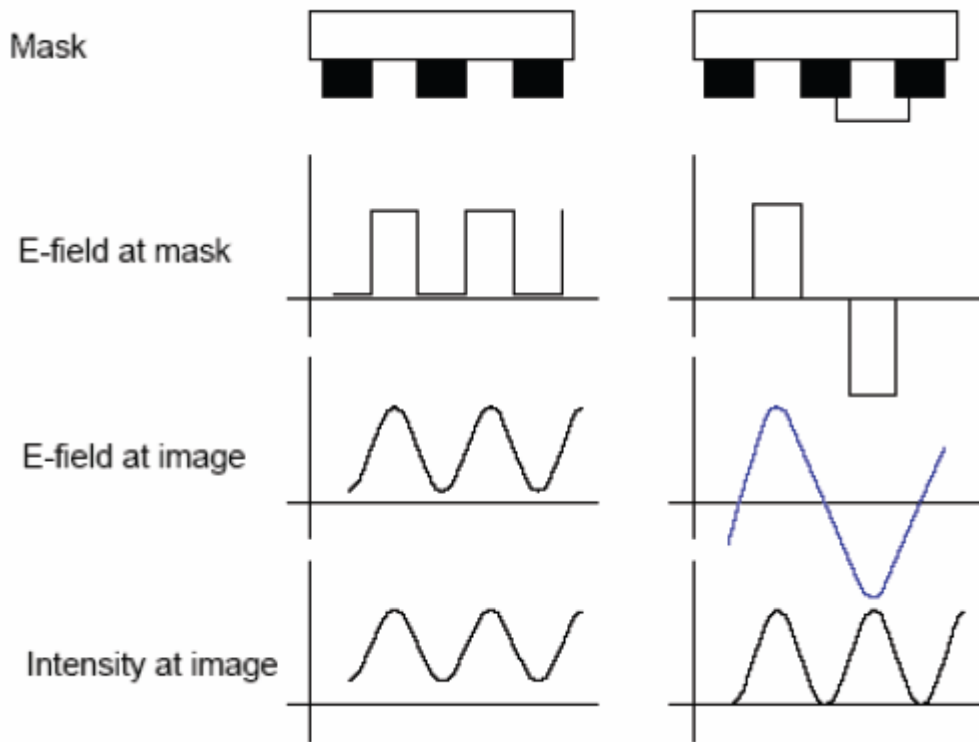


Fig 1-6 binary (Left) and Alternating Phase Shifting (Right)

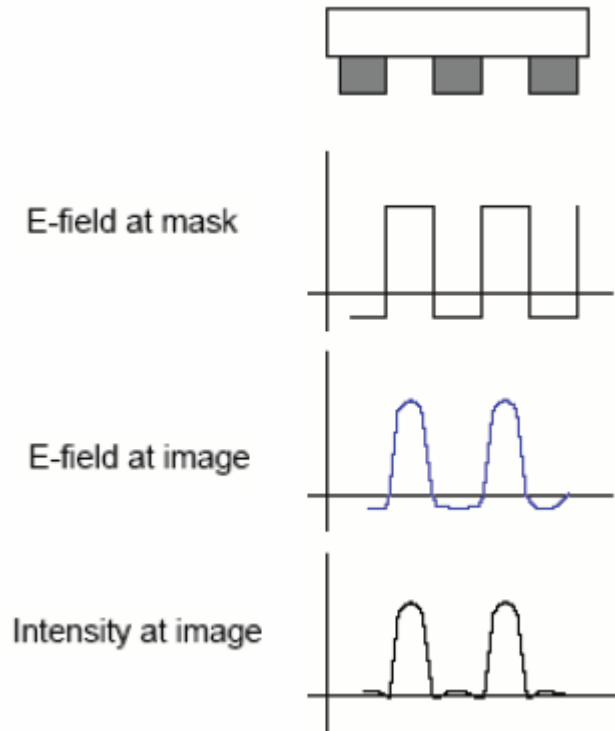


Fig 1-7 Attenuated Phase Shifting

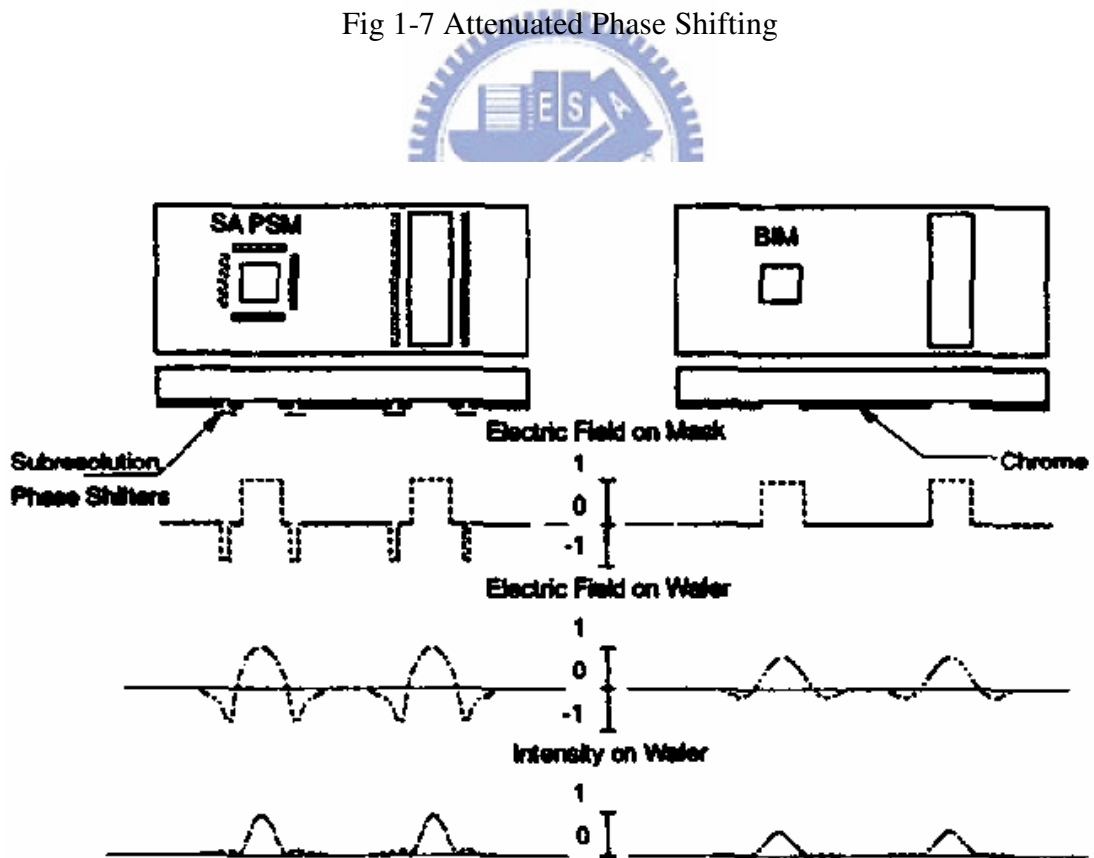


Fig 1-8 Subresolution-Assisted Phase Shifting [21]

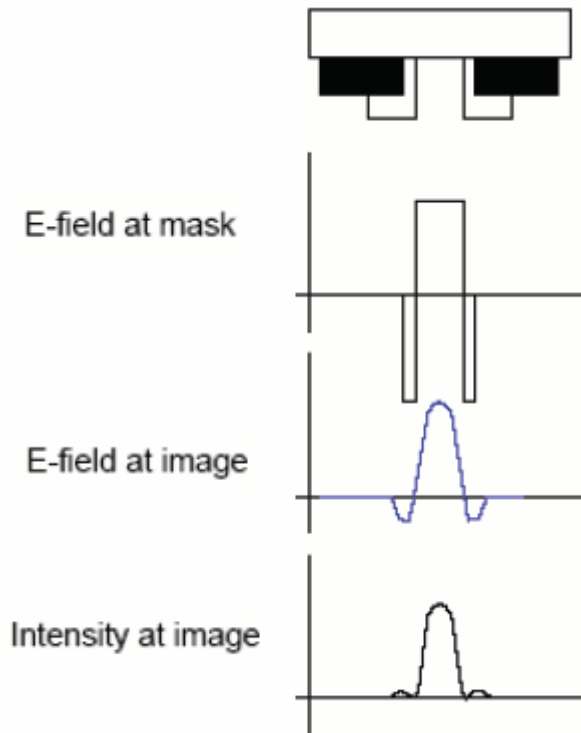


Fig 1-9 Rim Phase Shifting

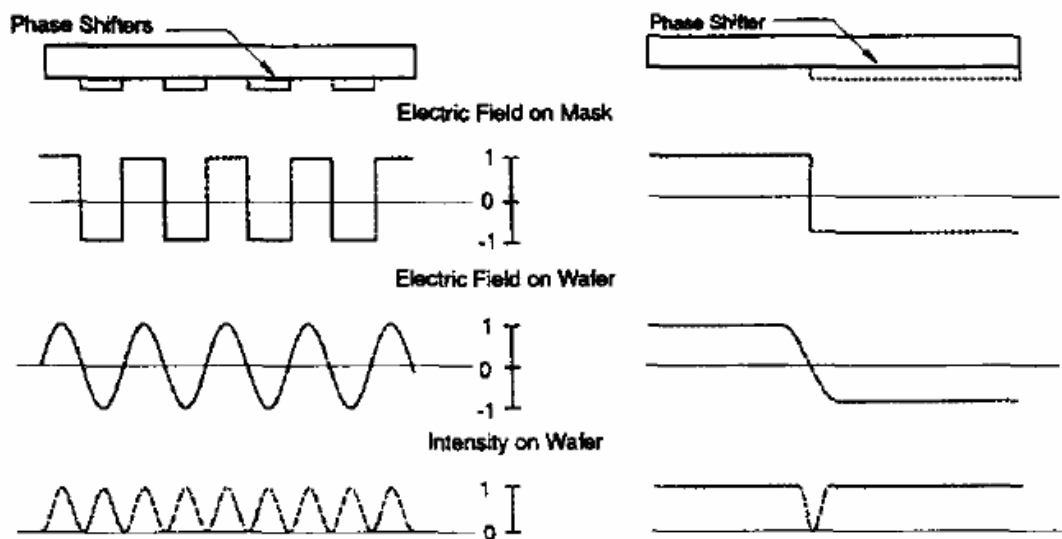


Fig 1-10 edge PSM [21]

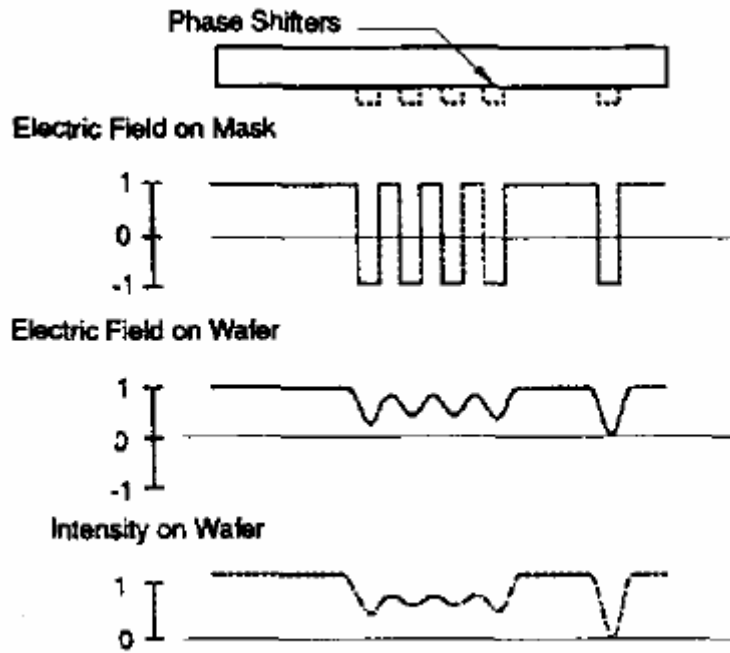


Fig 1-11 sub resolution Utt PSM [21]

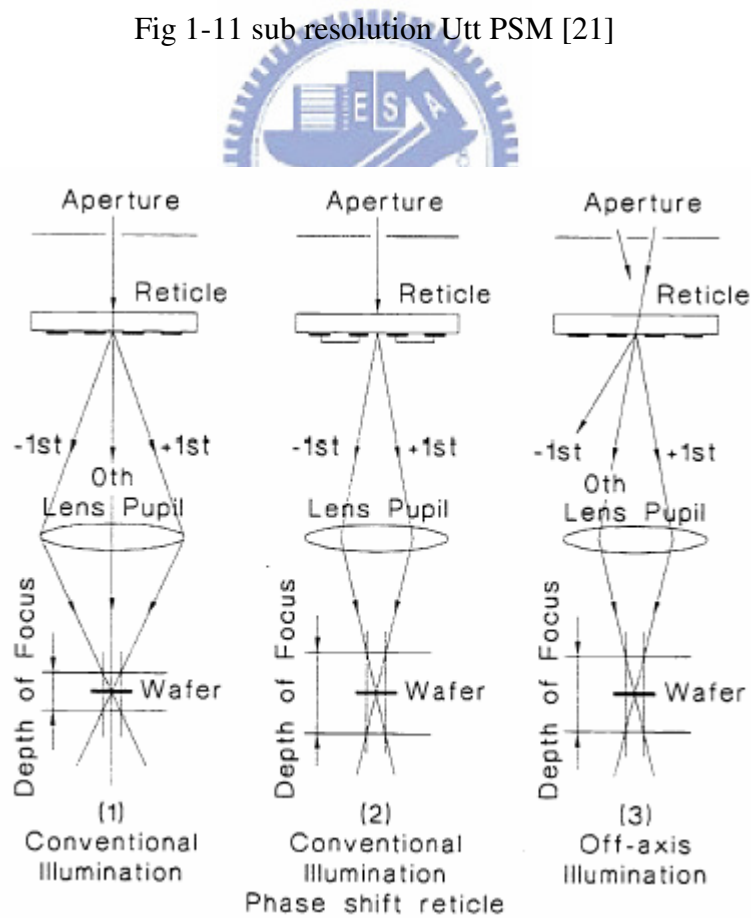


Fig 1-12 Two versus three beam imaging [26]

Chapter 2

Image Formation and Quality Parameter

2-1 Image formation in projection optics [28]

The projection system is composed of the illumination optics (light source and condenser lens), an object (mask), and the projection optics. The purpose of the illumination optics is to deliver light to the object with proper directionality and spectral characteristics that sufficient intensity and adequate uniformity across the field could be achieved. Since the source points are incoherent with one another, the resulting image is the incoherent sum of coherent images from each source point. We simplify the analysis of imaging process by assuming an on-axis, monochromatic point source to provide coherent illumination with wavelength λ . The projection optics is a system composed of several lens elements to achieve maximum field size with minimum aberration. It is convenient to approximate the image formation by a projection system in coherent light as a “double-diffraction” process. The mask, with a complex amplitude distribution $U_m(x,y)$ immediately behind it, produces by

diffraction a complex amplitude distribution $\widetilde{U}_m(f_x, f_y)$ in the pupil plane that is equal to the Fourier transform of $U_m(x,y)$,

$$\widetilde{U}_m(f_x, f_y) = F\{U_m(x, y)\} \quad (2-1)$$

The symbol F represents the Fourier transform operation, and f_x and f_y are the spatial frequencies of the object spectrum and are simply scaled coordinates in the pupil plane. The complex amplitude $\widetilde{U}_m(f_x, f_y)$ is frequently described as the complex diffraction pattern. The spatial Fourier component at (f_x, f_y) can be regarded as the magnitude of the plane wave propagating away from the mask plane with direction cosines

$$\sigma_x = \lambda \cdot f_x, \quad \sigma_y = \lambda \cdot f_y, \quad \sigma_z = \sqrt{1 - (\lambda f_x)^2 - (\lambda f_y)^2}$$

The light arriving at the pupil continues to form an image. Assume the projector is

diffraction limit and of unit magnification, the field distribution at the image plane

resulting from the ray $\widetilde{U}_m(f_x, f_y)$ is

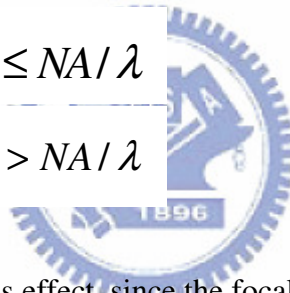
$$\widetilde{U}_m(f_x, f_y)e^{-i2\pi(f_x x + f_y y)}$$

where (x, y) are the image plane coordinates. This equation simply describes the propagation of a plane wave. The total effect is a sum of all the rays emitting from the entire pupil, which is a Fourier transformation again. Therefore, the basic equation for the calculating of electric field $U_i(x, y)$ at the ideal image plane is given by:

$$U_i(x, y) = F^{-1}\{\widetilde{U}_m(f_x, f_y)P(f_x, f_y)\} \quad (2-2)$$

Here an inverse Fourier transform operator F^{-1} instead of F is used to denote un-reciprocal spatial relation between the object plane and the image plane. The product of the pupil function P and the diffraction pattern stands for a circularly symmetric optical system typical in photolithography is defined as:

$$P(f_x, f_y) = \begin{cases} 1, & \sqrt{f_x^2 + f_y^2} \leq NA / \lambda \\ 0, & \sqrt{f_x^2 + f_y^2} > NA / \lambda \end{cases}$$



with the consideration of defocus effect, since the focal length is sufficiently large compared with the wavelength of light to validate the application of the stationary-phase approximation, the three-dimensional amplitude distribution of the image in the vicinity of the ideal image plane can be expressed by modifying Eq.(2-2) with an additional complex exponential term that demotes the phase variation due to defocus. The approximation yields

$$U_i(x, y, d) = F^{-1}\left\{\widetilde{U}_m\left(\frac{\sigma_x}{\lambda}, \frac{\sigma_y}{\lambda}\right)P\left(\frac{\sigma_x}{\lambda}, \frac{\sigma_y}{\lambda}\right)\exp\left(i\frac{2\pi}{\lambda}d\sqrt{1-(\sigma_x^2 + \sigma_y^2)}\right)\right\} \quad (2-3)$$

Here we use the direction cosine of the phase waves σ_x and σ_y instead of f_x and f_y to correlate the image formation with the plane wave propagation. The variable d specifies the defocus distance from the ideal image point. The aerial image is defined as the intensity distribution of the image and is simply the square of the magnitude of the electric field

2-2 Contrast [29-31]

Image contrast (Fig2-2) is defined in the conventional form

$$contrast = \frac{I_{max} - I_{min}}{I_{max} + I_{min}} \quad (2-4)$$

Where I_{max} and I_{min} are the maximum and minimum intensities in the aerial image respectively. Generally, high aerial image contrast can achieve better resist profiles. By increasing the optical contrast of the image, the quality of resist profiles can be improved. The aerial image contrast varies with NA and σ .

2-3 NILS (Normalized Image Log Slope)

It has been demonstrated that the normalized image log-slope (Fig 2-3) is a function well-suited to characterize the printability of given features:

$$NILS = w \left| \frac{1}{I} \frac{dI}{dx} \right| = w \left| \frac{d \ln I}{dx} \right| \quad (2-5)$$

where CD=critical dimension (line width), I=intensity, and x=length.

2-4 MEEF [32-34]

MEEF was defined as how reticle CD errors are translated into wafer CD errors and its expression is in the following way where M is the reduction ratio of the lens, usually 4.

$$MEEF = \frac{\Delta CD_{wafer}}{(\Delta CD_{mask}) / M} \quad (2-6)$$

2-5 Process window [35]

Since the effect of focus is dependent on exposure, the only way to judge the response of the process to focus is to simultaneously vary both focus and exposure in what is known as a focus-exposure matrix. Fig. 2-4 shows typical examples of the output of a focus-exposure matrix using linewidth, sidewall angle, and resist loss as the responses. The most common of these curves (Fig. 2-4a) is called the Bossung plot and shows linewidth versus focus for different exposures.

Of course, one output as a function of two inputs can be plotted in several different ways. And the most useful way to plot the two-dimensional data set of CD versus focus and exposure is a contour plot—contours of constant linewidth versus focus and exposure (Fig. 2-5). Obviously, sidewall angle and resist loss could also be

plotted in these alternate forms if desired.

The contour plot form of data visualization is especially useful for establishing the limits of exposure and focus which allow the final image to meet certain specifications. Because of the nature of a contour plot, other variables can also be plotted on the same graph. Figure 2-6 shows an example of plotting contours of CD (nominal $\pm 10\%$), 80° sidewall angle, and 10% resist loss all on the same graph. The result is a process window--a region of focus and exposure which keeps the final resist profile within all three specifications (shown as the shaded area of Fig. 2-6). The focus-exposure process window is one of the most important plots in lithography since it shows how exposure and focus work together to affect linewidth, sidewall angle and resist loss. All values of focus and exposure which lie inside the process window produce features which meet the profile specifications. All values of focus and exposure which lie outside the process window produce features which do not meet specifications.

Next we will find the maximum range of focus and exposure (that is, the maximum process requirement) that can fit inside the process window. A simple way is to graphically represent errors in focus and exposure as a rectangle on the same plot as the process window. The width of the rectangle represents the built-in focus errors of the processes, and the height represents the built-in exposure errors. Then we can find the maximum rectangle which fits inside the process window. As shown in Fig. 2-7a, there are many possible rectangles of different widths and heights which are maximum. Each maximum rectangle represents one possible trade-off between tolerance to focus errors and tolerance to exposure errors. Larger depth of focus can be obtained if exposure errors can be minimized. Likewise, exposure latitude can be improved if focus errors are small. The result is a very important trade-off between exposure latitude and DOF. Fig 2-7b shows an analysis of the process window where every maximum rectangle is determined and their height (the exposure latitude) is plotted versus their width (depth of focus).

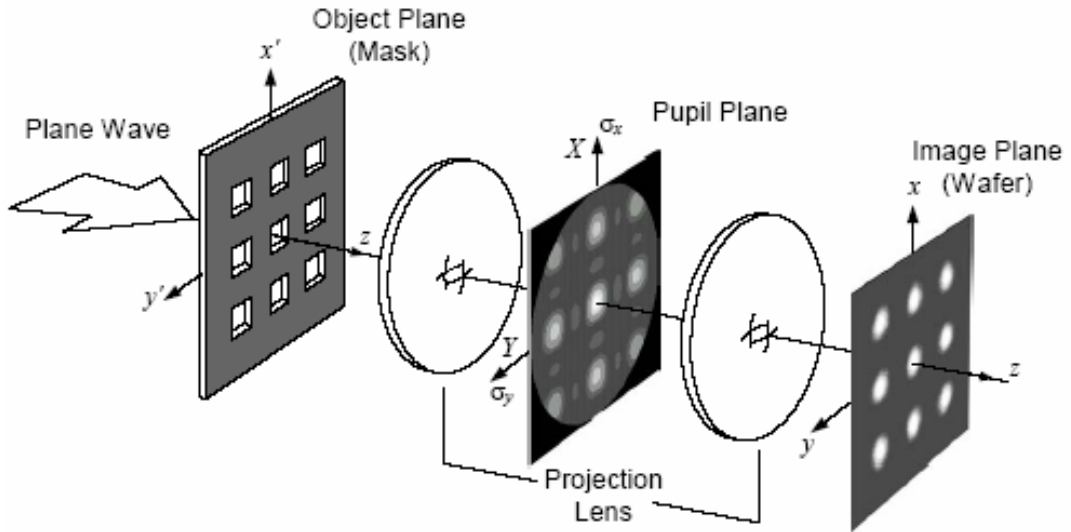


Fig 2-1 Schematic view of a generic projection system and principle of image formation

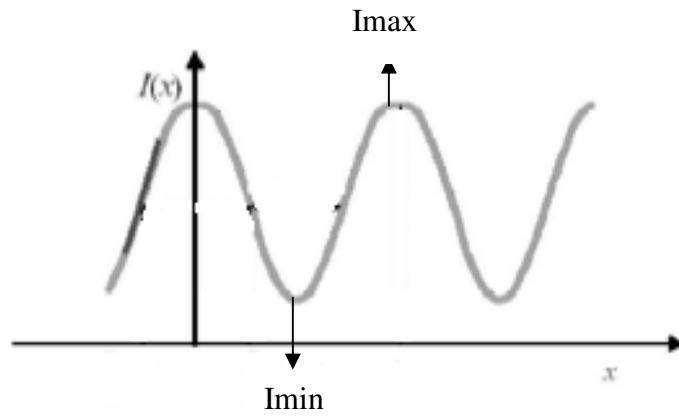


Fig 2-2 contrast

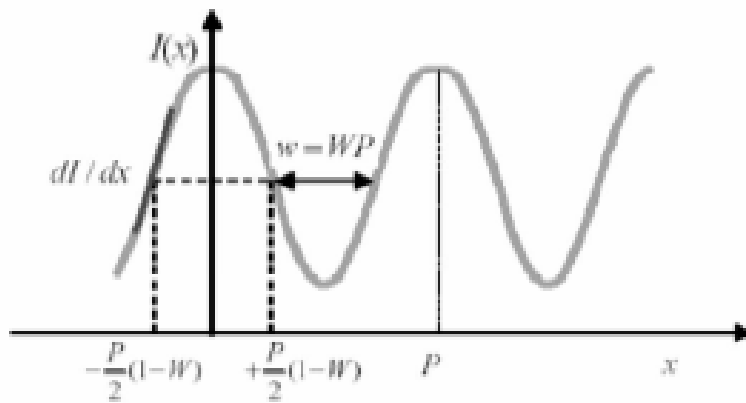


Fig 2-3 Normalized Image Log Slope

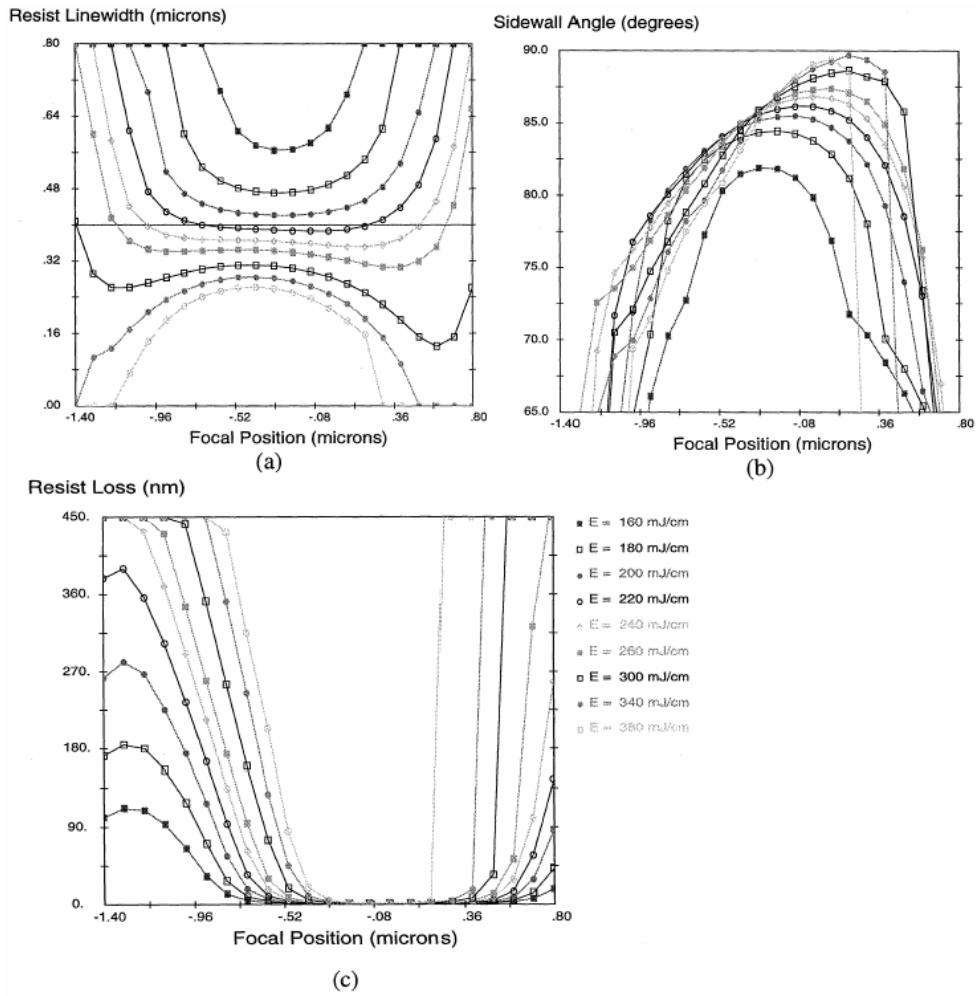


Fig 2-4 The effect of focus and exposure on the resulting resist profile: (a) linewidth, (b) sidewall angle, and (c) resist loss. [35]

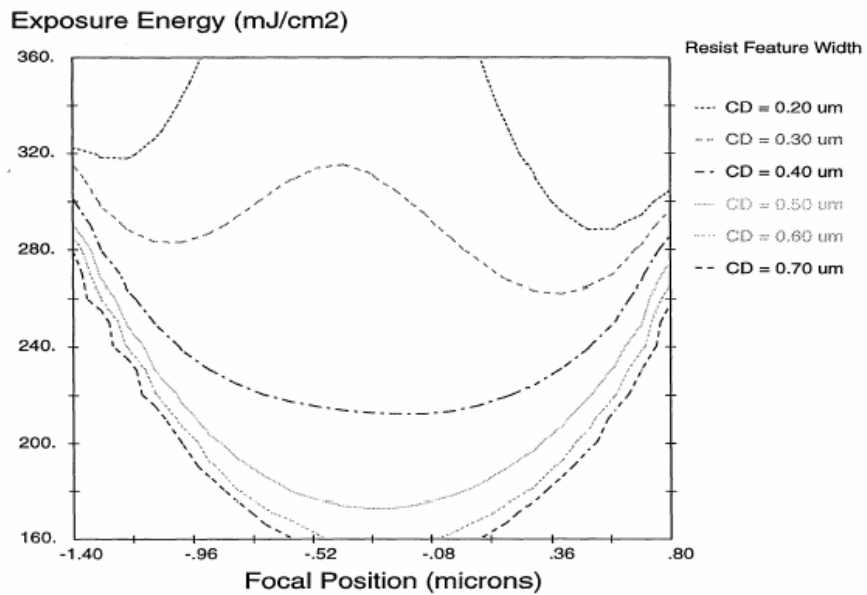


Fig. 2-5 contours of constant CD versus focus and exposure [35]

Percent Exposure Variation

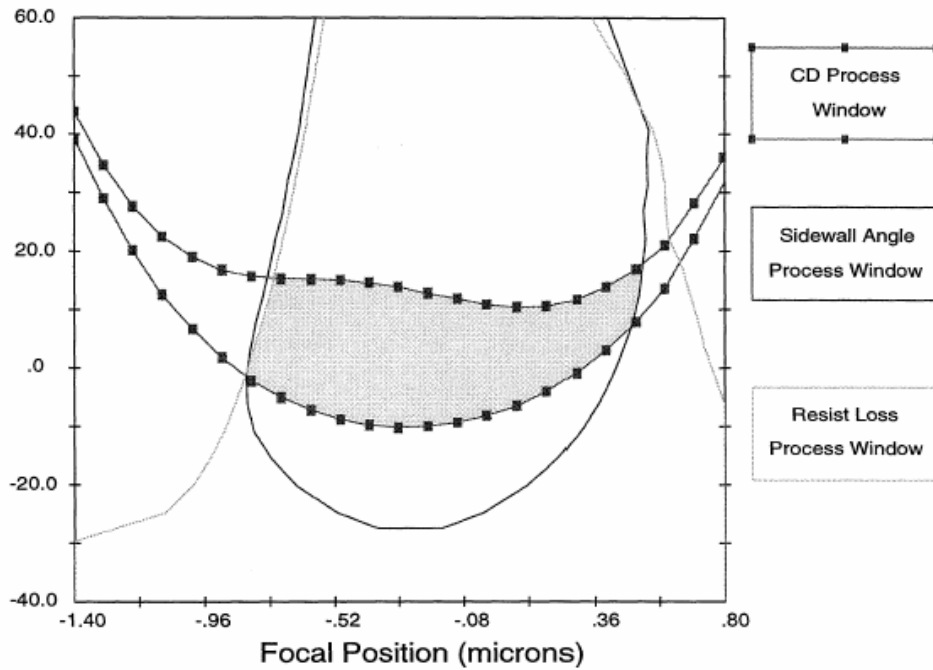
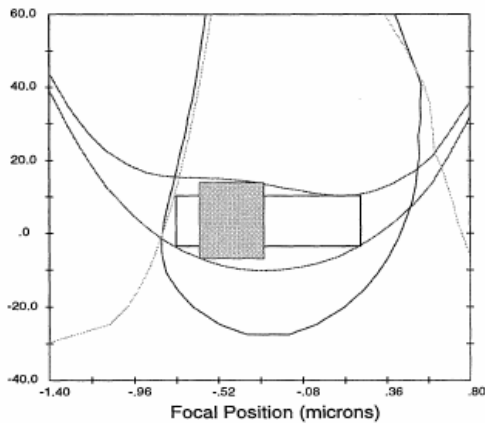


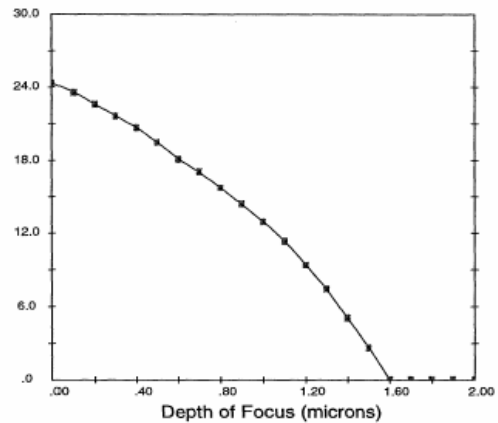
Fig 2-6 The focus-exposure process window constructed from contours of the specifications for linewidth, sidewall angle and resist loss. Shaded area the shows overall process window. [35]

Percent Exposure Variation



(a)

Percent Exposure Latitude



(b)

Fig 2-7 The process window (a) is analyzed by fitting all of the maximum rectangles, then plotting their height (exposure latitude) versus their width (depth of focus) as in (b) [35]

Chapter 3

Principle of Iso-Focal

3.1 Link between the iso-focal point and the DOF

3.1.1 Definition of the iso-focal point

The best contrast of the image is located at best focus. Around this point, the image degrades as a function of defocus. One of the characteristics of the intensity profile is that each of them cross at a same point called iso-focal point (figure 3-1). It is an invariant point in CD as function of defocus. At the best focus ($f=0\mu\text{m}$), the image contrast is the highest and this contrast decreases as function of defocus down to zero for the largest defocus. In this case, no image is formed.

3.1.2. Influence of the iso-focal position on the DOF

Practically, the depth of focus corresponds to the focus range where the image is considered to be acceptable. In terms of CD, it corresponds to a focus range where the CD is between +/- 10% of the target CD. Generally, for a given mask dimension, the target CD corresponds to the CD at the best focus. But the measured CD at each focus increases or decreases more or less rapidly depending on the position of the iso-focal point compared to the position of the target CD. This limits the depth of focus. DOF is maximum when the CD is invariant as function of defocus. This is only possible when the target CD is close to the iso-focal point.

In practice, the depth of focus is determined from the Bossungs curves, variation of the CD versus dose and focus. At first order, it is possible to fit this CD variation as a function of defocus, intensity threshold and position of the iso-focal point with this simple expression [36-37]:

$$CD = c_1(f-f_0)^2(t-t_0) \quad (3.1)$$

Where

c_1 : constant function of the process

f et f_0 : the position of the focus and the position of the best focus.

t et t_0 : the intensity threshold of the measured CD and the iso-focal intensity threshold.

From the expression (3.1), the depth of focus can be approximated by:

$$DOF = \frac{k}{\sqrt{|t-t_0|}} + \eta \quad (3.2)$$

Where

k et η : constants depending on the tolerance (+/-10% of the target CD) and the process

t et t_0 : the intensity threshold of the measured CD and the iso-focal intensity threshold.

This expression illustrates the fact that the DOF is closely linked to the position of the iso-focal point compared to the position of the target CD. When these two points are at the same level the depth of focus is maximum. Figure 3-2 shows the evolution of the iso-focal intensity threshold and the evolution of the depth of focus of a 150nm line as a function of the pitch with a 193nm wavelength and for an annular illumination. For a 1:1 feature (equal line and space) the iso-focal intensity threshold is at the same level as the intensity threshold of the target CD. Then the iso-focal intensity threshold increases to a constant value for isolated lines. The evolution of the DOF is function of the evolution of the iso-focal intensity threshold. It is maximum for the pitch 1:1 then it decreases when the iso-focal intensity threshold moves further from the threshold of the 1:1 pitch. DOF reaches a constant level when the iso-focal intensity threshold reaches its constant value for the isolated lines.

Generally for a given pitch and illumination conditions, the intensity threshold of the target CD is not at the iso-focal level. The aerial image being function of the mask dimension, illumination conditions (NA, σ) and resist parameters (resist thickness, contrast...), the intensity threshold of the target CD is also function of these same parameters. It is then possible to correct the position of the intensity threshold of the target CD and to have it overlapping with the iso-focal point.

3.2 Evolution of the iso-focal point

3-2.1 Theoretical background

Fig 3-3a shows a schematic sketch of a lithographic system. It consists of four parts: illumination optics, mask, projection optics and wafer. The light that falls onto the mask can be considered as a sum of plane waves with different angles of incidence. These plane waves are diffracted by the mask into the several directions. Here we will limit our study to the zero and first orders of diffraction (0, 1 and -1) because in the case of low k_1 imaging most of the contribution comes from these orders. We will consider only one-dimensional patterns.

A feature on a mask is reproduced on the wafer by a light interference process from the diffracted orders. Considering the coherence properties of lithographic light sources, we consider that two beams interfere if they come from the same source point. In the case where the feature pitch is small enough, as we can see in Fig 3-4, from the source S1, P_{-1} interacts with P_0 . The first-order contribution P_1 is not captured by the pupil. We have here only an interaction between two beams (-1 and 0). We have the same with another source point S2 where only P_0 and P_1 interact together because the pupil does not capture P_{-1} .

The iso-focal intensity threshold corresponds to the continuous component (background intensity) of the aerial image. The intensity expression of the aerial image can be obtained from the Fourier decomposition. We can then easily deduce the background intensity (zero order of the Fourier series of the aerial image) and thus also the variation of the iso-focal point. In the following, we will study the theoretical variation of the iso-focal intensity threshold for three types of masks: binary mask, alternated mask and attenuated phase shift mask.

3.2.2 Binary and attenuated masks [38]

Image formation using a binary mask or an attenuated PSM is shown in Fig. 3-5(a).

For a pattern with a pitch of $2L$ and aperture width of $2w$ (Fig. 3-5(b)), the amplitude at the

mask can be expressed as $T(x)=1$ for $|x| < w$, and $T(x)=t$ for $|x| > w$. The value of t represents the transmittance of dark region at the mask. The case of $t=0$ corresponds to a binary mask, and $t < 0$ indicates an attenuated PSM. For an opening ratio $\beta=w/L$ and fundamental frequency $f_0=1/2L$, the one-dimensional Fourier spectrum $F(f)$ of the binary mask or attenuated PSM is given as

$$F(f)=\{\beta+(1-\beta)t\}\delta(f-f^*)+\{(1-t)\sin(\beta t)/\pi\}\{\delta(f+f_0-f^*)+\delta(f-f_0-f^*)\} \quad (3.3)$$

and $C_0 = \beta + (1-\beta)t$; $C_1 = (1-t)\sin(\beta t) / \pi$

When the 0th, -1st, and +1st components are transmitted for the set of S_3 (Fig. 3-5(c)), the image at the wafer is formed by three-beam interference and its intensity is expressed as

$$I_1(X) = \{C_0 + 2C_1 \cos(2\pi X)\}^2 \quad (3.4)$$

Similarly, elimination of either the -1st or the +1st component for the case of S_2 gives

$$I_2(X) = C_0^2 + 2C_1^2 + 2C_1 C_0 \cos(2\pi X) \quad (3.5)$$

and the elimination of both the -1st and +1st components gives

$$I_3(X) = C_0^2 \quad (3.6)$$

Here, let A_3 be the source element ratio for three-beam interference, A_2 that for two-beam interference, and A_1 that for one beam transmission. The equation for defining the image width is then expressed with a certain threshold level I_{th} as follows.

$$A_3 \{C_0 + 2C_1 \cos(2\pi X)\}^2 + A_2 \{C_0^2 + C_1^2 + 2C_1 C_0 \cos(2\pi X)\} + A_1 C_0^2 = I_{th}$$

(3.7)

and $A_1 + A_2 + A_3 = 1$

The ratios A_3 , A_2 , and A_1 vary depending on both the fundamental frequency of a pattern f_0/f_C and the illumination conditions. For conventional circular illumination, five cases (Fig. 3-6) can be considered to find the A_3 , A_2 , and A_1 values. They are,

(a) for $f_0/f_C < (1-\sigma)$	$A_3 = 1$	$A_2 = 0$	$A_1 = 0$
(b) for $(1-\sigma) < f_0/f_C < (1-\sigma^2)^{0.5}$	$0 < A_3 < 1$	$0 < A_2 < 1$	$A_1 = 0$
(c) for $(1-\sigma^2)^{0.5} < f_0/f_C < 1$	$0 < A_3 < 1$	$0 < A_2 < 1$	$0 < A_1 < 1$
(d) for $1 < f_0/f_C < (1+\sigma)$	$A_3 = 0$	$0 < A_2 < 1$	$0 < A_1 < 1$
(e) for $(1+\sigma) < f_0/f_C$,	$A_3 = 0$	$A_2 = 0$	$A_1 = 1$

From equation 3.7, we can determine the intensity threshold of the iso-focal point.

It corresponds to the continuous components and is written as :

For a binary mask:

$$I_{iso-focal} = \beta^2 + \frac{A_2}{\pi^2} \sin^2(\pi\beta) = I_\beta + I_{A_2} \quad (3.8)$$

For attenuated PSM mask:

$$I_{iso-focal} = (\beta + (1-\beta)t)^2 + \frac{A_2}{\pi^2} ((1+t)\sin(\pi\beta))^2 \quad (3.9)$$

The threshold of the iso-focal point is mainly a function of the mask aperture ratio (β)

and A_2 (area of the diffracted waves participating to the 2 wave interferences). A_2 is a function of pitch and illumination (conventional, annular and quadripole).

3.2.3 Alternated PSM masks

Image formation using an alternating PSM is shown in Fig. 3-7(a). Here, the period of the amplitude transmittance at the mask is $2L$, the aperture width is w (using 1X

dimensions for notation), and an opening ratio β is defined as w/L . This amplitude at the

mask can be expressed as $T(x)=1$ for $|x| < w/2$, $T(x)=-1$ for $|x| > L-w/2$, and $T(x)=0$ for other x (Fig. 3-7(b)).

The imaging characteristics of the one-dimensional patterns treated here are estimated by considering one-dimensional diffraction. The plane wave passing through the alternating PSM is diffracted and forms a pair of -1st and +1st order and higher order diffracted waves. Therefore, the Fourier transform $F(f,g)$ of the one-dimensional alternating PSM can be replaced by $F(f)$, and expressed as

$$F(f) = (2/\pi) \cos\{\pi(1-\beta)/2\} \times \{\delta(f+f_0/2) + \delta(f-f_0/2)\} + \dots \quad (3.10)$$

where f_0 is the fundamental frequency of the line patterns. The one-dimensional image formed by a source element is rewritten as

$$I(x) = \left| \int F(f-f') K(f) \exp(2\pi j f x) df \right|^2 \quad (3.11)$$

where f' indicates the source image position in the f direction at the pupil plane of the projection lens and is equivalent to the local position in the 1st or -1st diffracted wave as shown in Fig. 3-7(c).

When the pair of components of $f = f_0/2$ and $-f_0/2$ indicated as S_2 can pass through the lens the image is formed by two-beam interference and its intensity distribution (eq. (3.11)) is expressed as

$$I_1(x) = (8/\pi^2) \cos^2\{\pi(1-\beta)/2\} \times [1 + \cos\{2\pi f_0(x+2Df')\}] \quad (3.12)$$

where D is a parameter in proportion to defocus. Assuming the case of the best focal plane,

i.e., $D=0$, the point source position f' is eliminated in eq. (3.12). Therefore, intensity distribution is simplified as

$$I_1(x) = (8/\pi^2) \cos^2\{\pi(1-\beta)/2\} \{1 + \cos(2\pi X)\} \quad (3.13)$$

where $X = f_0 x$

On the other hand, when only one component passes through the lens, indicated

as S_1 in the shaded region in Fig. 3-7(c), the image intensity is given as

$$I_2(x) = (4/\pi^2) \cos^2\{\pi(1-\beta)/2\} \quad (3.14)$$

The image intensity at the wafer is obtained by summing up the results given by eqs. (3.13) and (3.14) with the results weighted according to the number of corresponding point source elements. Let A be the ratio of point sources for two-beam interference to the total number of point sources; $(1-A)$ is then the ratio of point sources for one component elimination.

Using the ratio A , the equation defining the image width is expressed with a certain threshold level I_{th} as follows.

$$A(8/\pi^2) \cos^2\{\pi(1-\beta)/2\} \{1 + \cos(2\pi X)\} + (1-A) (4/\pi^2) \cos^2\{\pi(1-\beta)/2\} = I_{th} \quad (3.15)$$

In the same way as before, from the expression of the aerial image intensity, we can determine the evolution of the iso-focal intensity threshold for alternated PSM masks.

It is given by the following expression

$$I_{iso-focal} = (1+A) \left(\frac{4}{\pi^2}\right) \cos^2\left[\frac{\pi(1-\beta)}{2}\right] \quad (3.16)$$

where

A : the area of the orders contributing to the interferences (normalized by the area of the source)

$\beta = w/p$: the mask aperture rate

w : mask aperture width

p : pitch

The theoretical evolutions of the iso-focal intensity of a 150nm line with the 3 types of masks studied before are presented in figure 3-8. These 3 expressions are obtained from the expressions (3.8), (3.9) and (3.16). For the attenuated mask, the transmission is fixed at 10% ($t=0.1$). In each case, we have used a conventional illumination $\lambda=193\text{nm}$, $NA=0,63$ and $\sigma=0,8$. The theoretical evolutions show that in the three cases the iso-focal variation is the same: abrupt increases for the dense pitches, low increase for semi-dense pitches and isolated lines. The difference in term of threshold level between dense and isolated lines is more important with alternated PSM mask (around 0.6) than with the binary masks (0.5) or attenuated (0.4).

3.3 Analysis of the iso-focal variation

The expressions (3.8) and (3.9) show that the iso-focal intensity threshold varies

mainly as a function of the transmission rate (β) and the area of A_2 (area of the 2 wave interference). So we will compare the evolution of the iso-focal threshold of I_β and I_{A_2} (terms of the expression (3.8)) where I_β is mainly function of β and I_{A_2} function of A_2 , and then see where are the predominant areas of these two parameters (β and A_2) influencing the position of the iso-focal point. Figure 3-9 shows this comparison for a 150nm line obtained with conventional illumination. I_β increases in function of the space to line ratio. Below the ratio 0.2, there is no 2 wave interference (1 and -1 orders are not captured by the pupil plane). In the dense lines area (between 0.2 and 1), I_{A_2} increases until reaching a maximum value (for the ratio of 1). Then, it decreases until the isolated lines where we have any interference. From this curve, we can distinguish two regions. For any ratio of space/line above 3 or below 0.2, I_β can be considered as predominant. The iso-focal intensity threshold varies then mainly as a function of β . Between 0.2 and 3, I_{A_2} is not negligible. The iso-focal intensity threshold is then function of the two parameters β and A_2 . In the range where the iso-focal point is mainly function of β , any variation of the line will change the β value and consequently the iso-focal threshold level. That is the reason why we observe an increase of the threshold when we decrease the line width.

3.4 Improvement of the DOF

The intensity threshold position of the iso-focal point compared to the threshold position of the target CD is a fundamental parameter in the improvement of the DOF. The closer the iso-focal point will be to the target CD, the larger the DOF will be. A solution to improve the DOF for all structures on a circuit will be to decrease the iso-focal intensity threshold of the semi-dense and isolated lines to the same level of the critical structures (which are generally the more dense lines).

The solution is to add assist features. The dimension of these assist features determines the transmission of the light and so the iso-focal intensity threshold. For example, the iso-focal intensity threshold of a 150nm line with a pitch of $0,3\mu\text{m}$ is around 0,35 ($\beta=0,5$). For the same lines placed in a semi dense lines with a pitch of $0,5\mu\text{m}$, the iso-focal threshold level is at 0,6 ($\beta=0,7$). The addition of assist features of 70nm besides the main lines decreases this transmission rate to 0,5 and so bring down the iso-focal intensity threshold of the semi dense lines to the level of the iso-focal threshold of the more dense lines (at 0,35). We can adjust the iso-focal intensity threshold of any line of a circuit by adding around the lines the corresponding assist features. The iso-focal intensity threshold of any pitch can then be at the same level of

the more dense lines. The depth of focus will be close to the DOF of the more dense lines.

Figure 3-10 shows the evolution of the iso-focal intensity threshold of a 150nm line (binary mask) obtained with a simple exposure, with 50nm sub resolution assist features (SRAF) and with a watching of the size of the assist features to the corresponding pitch (described in the figure by CODE). At the simple exposure dose, the iso-focal level increases from the dense to the isolated lines. The difference between the iso-focal threshold of the dense lines and the one of the isolated lines is around 0,3. This large difference induces a large difference in terms of DOF. With 50nm SRAF, the iso-focal intensity threshold of the isolated lines decreases by 50% compared to the iso-focal intensity threshold of the dense lines. Nowadays, this solution of SRAF is largely used by the integrated circuit manufacturers for the production of the 90nm and 65nm devices. This improves the DOF of the semi-dense and isolated lines but it does not fully maximise the DOF as the iso-focal intensity threshold is still at a high level. The best solution for optimizing the iso-focal intensity threshold is to add around each line the proper assist features (larger assist features). The iso-focal intensity threshold of each line will be then close to the iso-focal intensity threshold of the dense lines. With this solution, the difference between the iso-focal intensity threshold is then less than 0,1. The DOF of the iso lines is very close to the DOF of the dense lines.

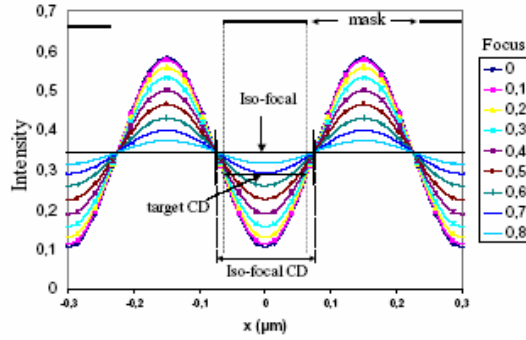


Fig. 3-1 Position of the iso-focal point in the aerial image curves. $CD(\text{mask})=0.12\mu\text{m}$; $p=0.30\mu\text{m}$, $\lambda=193\text{nm}$, $NA=0.63$ and $\sigma=0.5/0.8$ (annular illumination)

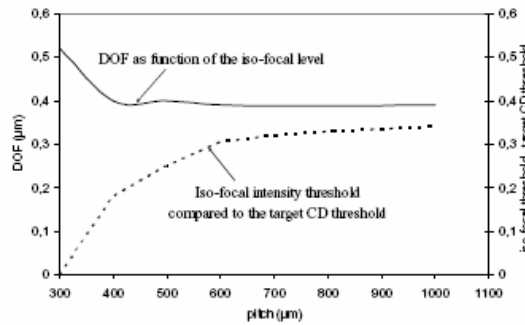


Fig. 3-2 Position of the iso-focal point compared to the target CD and the corresponding DOF as function of the pitch. $CD(\text{mask})=0.15\mu\text{m}$; $p=0.30\mu\text{m}$, $\lambda=193\text{nm}$, $NA=0.63$ and $\sigma=0.5/0.8$ (annular illumination)

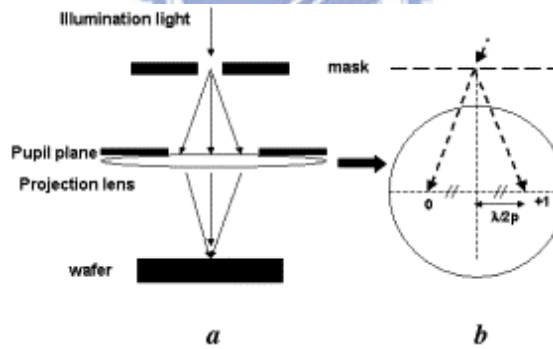


Fig 3-3 Schematic sketch of a lithographic system.

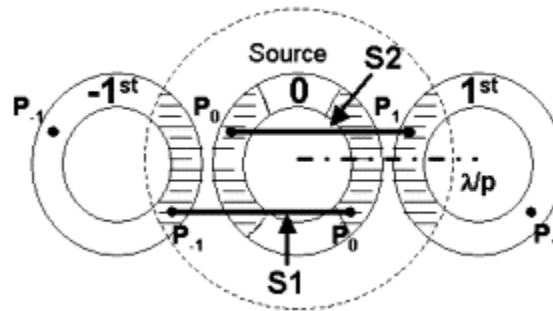


Fig 3-4 Diffracted waves captured by the pupil plane

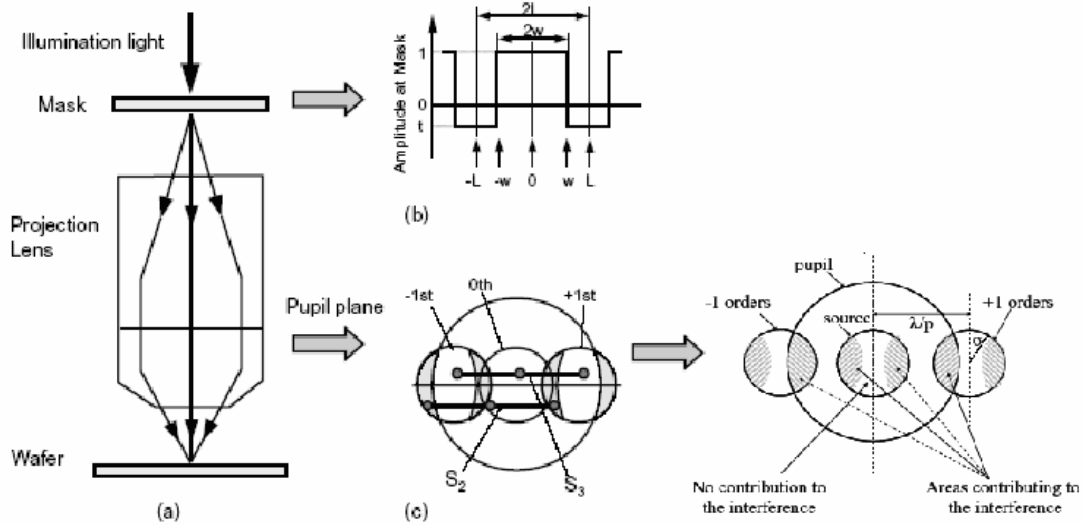


Fig. 3-5 Binary mask or attenuated phase shift mask imaging for periodic line patterns: (a) schematic structure of exposure optics, (b) transmitted amplitude of light at mask, (c) diffracted waves for partially coherent light. [41]

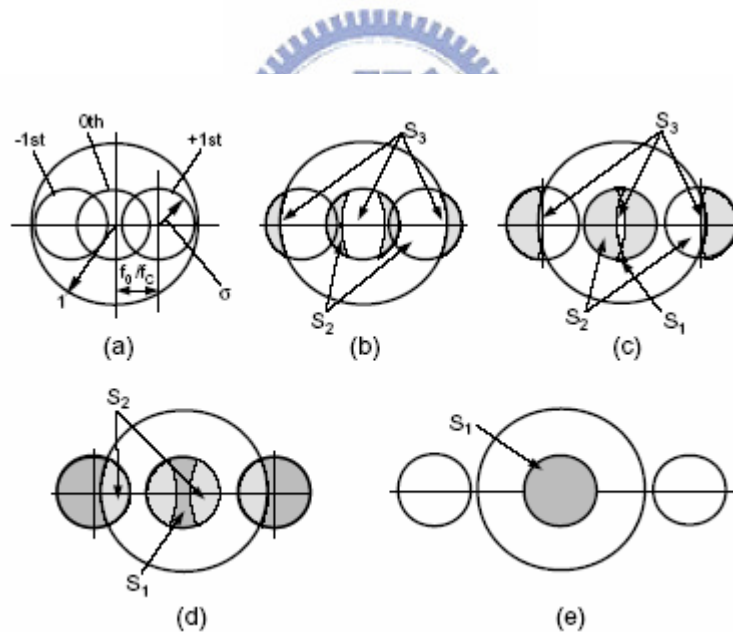


Fig 3-6 Diffracted waves of periodic line patterns for partially coherent light when (a) all components (-1st, 0th, and +1st) are transmitted, (b) either the -1st or +1st component is eliminated for some point sources, (c) both the -1st and +1st components are eliminated for some point sources, (d) some pairs of -1st and 0th components, or of 0th and +1st components are transmitted, (e) both the -1st and +1st components are completely eliminated. The areas denoted as S_3 , S_2 , and S_1 correspond to the source area for three-beam interference, two-beam interference, and only 0th order wave transmission. [41]

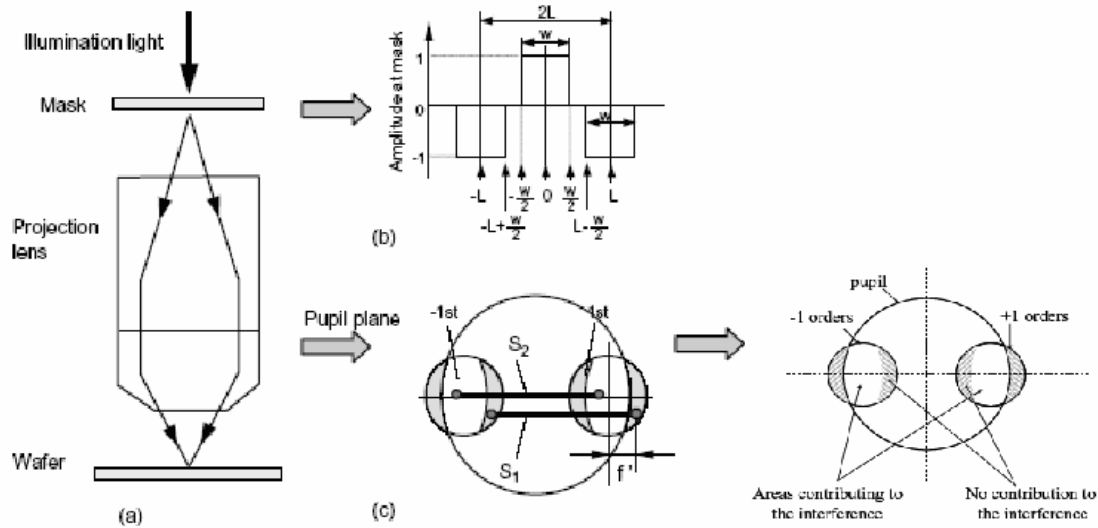


Fig. 3-7 Phase-shift mask imaging for periodic line patterns: (a) schematic structure of exposure optics, (b) transmitted amplitude of light at mask, (c) diffracted waves for partially coherent light [41]

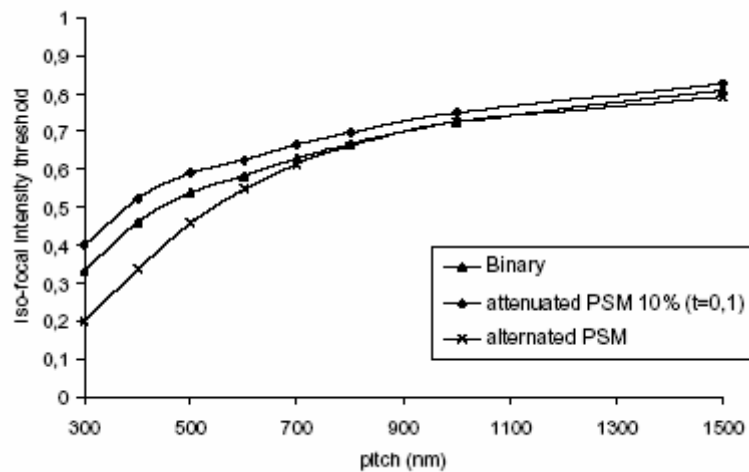


Fig. 3-8 The theoretical evolution of the iso-focal intensity threshold of a 150nm line with a conventional illumination ($\lambda=193\text{nm}$, $\text{NA}=0,63$ and $\sigma=0,8$) as a function of the pitch for three types of masks: binary, 10% attenuated PSM and alternated PSM

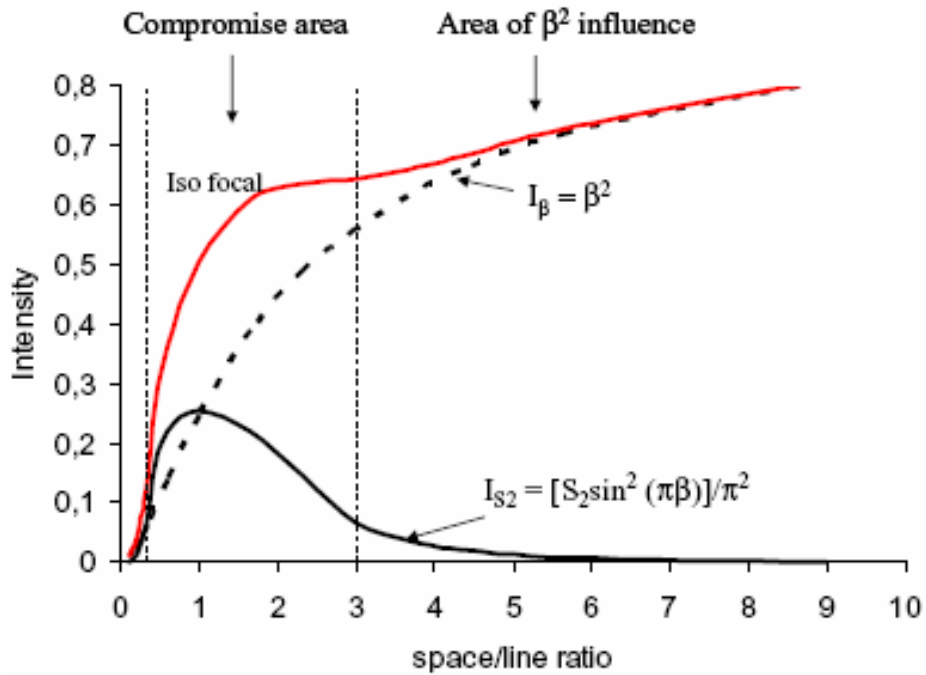


Figure 3-9 Evolution of I_β et I_{S_2} for a 150nm (binary mask) with a conventional illumination ($\lambda=193\text{nm}$, $\text{NA}=0.63$ and $\sigma=0.80$). S_2 is the normalized area of the two orders interference

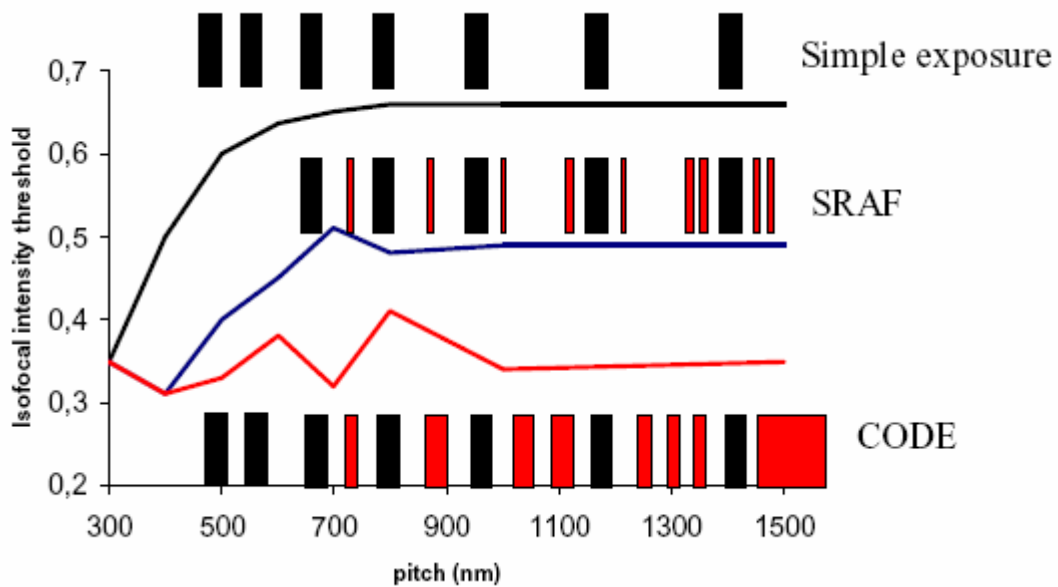


Fig. 3-10 Evolution of the iso-focal threshold of a 150nm line as function of the pitch with the simple exposure, SRAF (sub resolution assist features) and the CODE techniques using a conventional illumination ($\lambda=193\text{nm}$, $\text{NA}=0.63$ and $\sigma=0.8$).

Chapter 4

Principle and Simulation

4-1 The use of pair of bright lines

4-1.1 Concept of pair of bright lines

Fig. 4-1 shows an original mask for the formation of dark lines. But from the phenomena described in the last chapter, we can find the fact that a dark line image between a pair of bright lines would get the better CD-Focus characteristics. Because of this reason, we change the original dark line mask (Fig. 4-1) into another kind of dark line mask pattern in which we let the dark line surrounded by two thin bright lines such as schematically shown in Fig. 4-2. But when we use this kind of mask, in this pair of bright lines mask undesirable dark line is inevitably formed between adjacent pairs, so another time of exposure is necessary to erase the undesirable part by using a mask for 2nd exposure such as schematically shown in the lower part of Fig. 4-2.

Figure 4-3 shows optical image intensity profiles for a mask pattern of pair bright lines taking focus offset as a parameter. In the mask, 170 nm two bright lines are laid out with the separation of 170 nm in dark field. The distance between the pairs is 870 nm. Mask is CoG. In the graph, size and position of mask dark line between bright lines is schematically shown for comparison with formed images. As can be seen in the graph, iso-focal characteristics are observed in the image. If the effective image contrast is sufficiently high for resolution, very fine line pattern should be formed by the application of this image.

In Figure 4-4, the same image intensity profile is shown in detail by changing axis scale. In the graph, iso-focal slice level intensity (solid line) and intensity level which mediates resolution criteria (broken line) are shown with thick lines. The resolution criteria intensity is defined as 1/1.3 times of the slice level intensity. By this definition, the image which has the darkest intensity smaller than this resolution criteria intensity can be resolved as a line pattern with high contrast positive tone

resist. According to criteria, this image can be printed with CD and resolution DOF of $\sim 1.0\mu\text{m}$. The iso-focal width of the image, which is shown in the figure, is $\sim 90\text{ nm}$.

This mask pattern is effective to form a fine dark line even in the case of conventional illumination. Figure 4-5 shows calculated image intensity profiles under conventional illumination. The mask pattern is the same as that in Fig. 4-3. Optical conditions are $\text{NA}=0.60$, $\sigma=0.85$. Even with the conventional illumination, iso-focal CD of $\sim 140\text{ nm}$ is obtained. Also, resolution DOF of $\sim 1.0\mu\text{m}$ should be obtained in the meaning of effective image contrast. In the case of isolated bright line pattern, the minimum iso-focal CD is estimated to be $\sim 200\text{ nm}$ by a strong modified illumination even with the realizable high NA stepper in KrF wavelength. Thus, it should be worth surprising that $\sim 150\text{ nm}$ width image with iso-focal CD characteristics is formed with conventional imaging technique. As a consequence, isolated pattern and conventional large pattern can be formed in the same exposure by this method. As this case uses conventional illumination, pattern versatility should be high. Thus, this method is considered useful for gate a pattern printing for general logic devices.

4-1.2 The effect of the width of the bright lines on the image

In the following we will simulate how large of the width of the bright lines pair would get the best CD-Focus characteristics. Fig. 4-6 shows variation of image intensity profiles with changing the bright line width on the mask. The width is changed from 190 nm , 170 nm , to 150 nm . By changing the bright line width, iso-focal slice level is significantly varied. Therefore DOF is drastically changed with the mask bright line width. With large width bright line, iso-focal slice level becomes large and corresponding iso-focal CD is increased. In the case of smaller mask width, iso-focal slice level becomes smaller and Iso-focal CD becomes small. But, in this case, effective image contrast also becomes low resulting in poor resolution.

4-1.3 The effect of the width of the dark line on the image

Figure 4-7 shows the variation of optical image intensity profile with changing dark line width on mask. The width is changed from 190 nm , 170 nm , to 150 nm . In contrast with Fig. 4-6, iso-focal slice level is slightly changed with the dark line width. As a consequence, CD-Focus characteristics are not significantly varied with the dark line width. By increasing the dark line width, iso-focal CD becomes large and effective image contrast becomes high. On the contrary, by decreasing the dark line width, iso-focal CD is decreased and effective image contrast is also decreased. As a result, resolution of such image becomes difficult due to low effective contrast.

According to the results shown above, in the design of device pattern mask, pair bright lines with almost the same width should be applied within one layer. By this procedure, good CD-Focus characteristics should be obtained for wide range of line width.

4-1.4. Image formation with Att-PSM

Figure 4-8b shows image intensity profiles in the application of atten-PSM whose transmission is 6%. In comparison with the binary central line (Fig. 4-8a) which has image dimension=60nm DOF=0.9573 μ m, it shows that when change the central dark line to 6% attenuated PSM we can get a better image line width of 50nm with large DOF=0.9279 μ m . From these results shown above, it is found that we can improve the line image characteristic by changing the central dark line to an attenuated PSM.

4-2 Change the dark line between the pair lines with Atten-NPS

4-2.1 Concept of the use of Atten-NPS

In this section, imaging scheme of the same as before but replace the dark line between the pair of bright lines with Atten-NPS will be shown. In Fig.4-9, typical mask patterns (Top), optical image profiles (Middle) and these details (Bottom) in isolated line formation are shown for the former work (A) and for the improved one which will be discussed in this section (B), respectively. A quadrupole illumination with a specific incident angle is applied throughout this work. The configuration of illumination is essential.

In the former work, a pair of bright lines is delineated in binary mask or Atten-PSM. When this mask pattern is illuminated by the quadrupole illumination, very sharp dark line image is formed at center of the pair. As can be seen in the left bottom graph, a fine resist line with width of smaller than 50 nm can be formed by this image. However, as shown in a left middle graph, the outside of the pair becomes deeply dark due to large opaque area or phase compensation at an edge of Atten-PSM. Then, in developed resist pattern after an exposure of this image, the dark areas are resolved resulting in generation of undesirable patterns. To erase these undesirable resist patterns, appropriate light dose for this area by an additional exposure with an additional mask is necessary. Hence, in an application for an actual device pattern formation, double exposure is inevitable in the former technique.

In the top part of Fig.4-9 (B), a typical mask pattern for isolated line formation in the advanced one is shown. Mask pattern layout is very similar to that of the former work, but the outside of the pair of bright lines is composed with attenuating non-phase-shifting (Atten-NPS) area, while this area is completely opaque or phase-inverted attenuating in the former work. By this Atten-NPS whose transmission is 10~30%, the minimum image intensity at the outside becomes much higher than that in the central fine dark image. In the case of Fig. 4-9 (B), slice level is set at ~0.06. This is larger than the twice of the minimum intensity of the central fine line image, but is lower than one third of the minimum intensity at the outside area, which is ~0.18. As a result, when exposure dose is set at the appropriate value, only the central dark line can be resolved in a resist. The performance of fine isolated line formation seems a little poorer than that in the former work. But as seen in the bottom of Fig. 4-9 (B), ~50nm line can be formed with a large DOF.

4-2.2 Simulation of the advanced one with binary mask

In this section, imaging performance of the advanced one with binary mask will be discussed in detail. Fig. 4-10 shows the mask of changing the transmission of Atten-NPS area of isolated line. And in Fig. 4-11 shows the simulated results of aerial image for changing the transmission of Atten-NPS area from 20% to 30%. And in Fig. 4-12 shows the simulated results of process window for changing the transmission of Atten-NPS area from 20% to 30%. In graphs, aerial image profiles are plotted taking focus as a parameter. Optical conditions are quadrupole illumination with dark line width=170nm, the pair of bright line width=90nm, pitch=770nm, and transmission of the Atten-NPS with 20% (upper), 25% (middle), to 30% (lower), respectively.

From the results of simulation, we can see that, for variation transmission of Atten-NPS, the image line width is 80nm, 90nm, and 100nm for 20%, 25%, and 30% transmission of the Atten-NPS respectively. This result is due to the reason that for the lower transmission of the Atten-NPS, it is more similar to the opaque one which has the better image performance than the clear one. So it has the smaller image line width than the one which has higher transmission of the Atten-NPS that is more similar to the clear one.

4-2.3 Compare of the use of 6% and 20% Atten-NPS

In this section, similar analysis of former will be carried out. We will replace the

central dark line of the mask patterns with 6% and 20% transmission Atten-PSM, respectively. And in Fig. 4-13 shows the simulated results of aerial image for changing the transmission of Atten-NPS area from 20% to 30%. And in Fig. 4-14 shows the simulated results of process window for changing the transmission of Atten-NPS area from 20% to 30%. In graphs, aerial image profiles are plotted taking focus as a parameter. Optical conditions are quadrupole illumination with dark line width=170nm, the pair of bright line width=90nm, pitch=770nm.

By application of high transmission Atten-PSM for the central line on mask, imaging becomes like as those by Cr-less phase shift mask. Due to phase compensation, image intensity for the central line becomes very low resulting in finer line formation. But, when isolated line is formed with very fine width by application of high dose, formation of dense lines in the same exposure should become difficult because of high MEEF. Here, only imaging characteristics of isolated line will be discussed. Fine dark line image with superior focus characteristics is formed at the center.

4-3 Change the Atten-NPS with binary mask

In this section, we will use another method which use only the binary mask and need only one time exposure to gain the same result as former discussed.

When a pattern pitch is smaller than resolution limit of a projection optics, that is, the pitch is smaller than $0.5 NA/\lambda$, information of fine structure is not transferred to the image. And in order to let the opaque region of Fig 4-2 to be a partial clear region, so we change the opaque region to be a set of binary mask. But in order to prevent forming line image between this region, so we choose the thin line which is about 67nm which is so small for the resolution limit so it will not be printed. And then we can modulate the space between the thin dark lines to gain an appropriate transmission between the opaque region. In Fig 4-15 we can see that for a mask which is composed with 67nm lines and with pitch=140nm can has the similar aerial image with the mask which is 25% Atten-NPS. So we can change the opaque region of Fig 4-2 to be the binary mask and we can thus get the similar result as that of 25% Atten-NPS. From the aerial image and the process window for the simulation result shown in Fig 4-16 and Fig 4-17, we can prove that the method is useful.



Fig. 4-1 original mask for the formation of dark lines

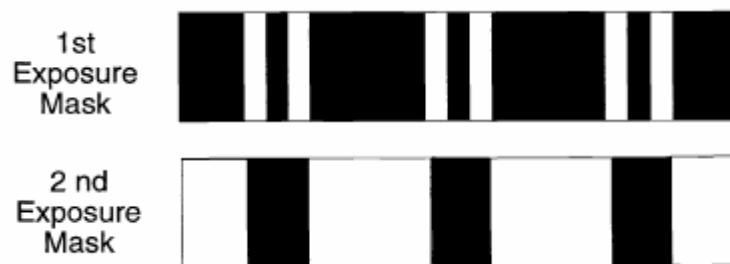


Fig. 4-2 Schematic mask pattern for this pattern formation method. Upper shows for fine dark line image formation and lower shows a mask for 2nd exposure to erase undesirable dark line pattern between the pairs of bright lines.

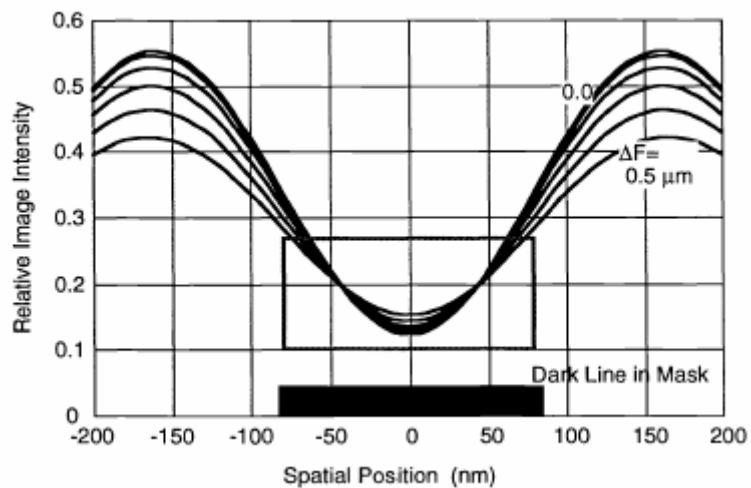


Fig. 4-3 Image intensity profiles of a bright lines pair mask pattern. CoG mask, NA=0.65.

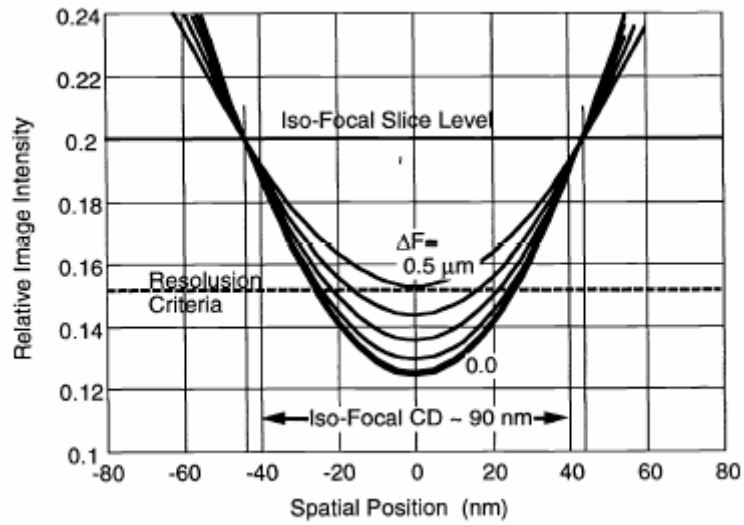


Fig. 4-4 The same image intensity profile as in Fig. 5 in large scale to appear the effective image contrast with focus offset.

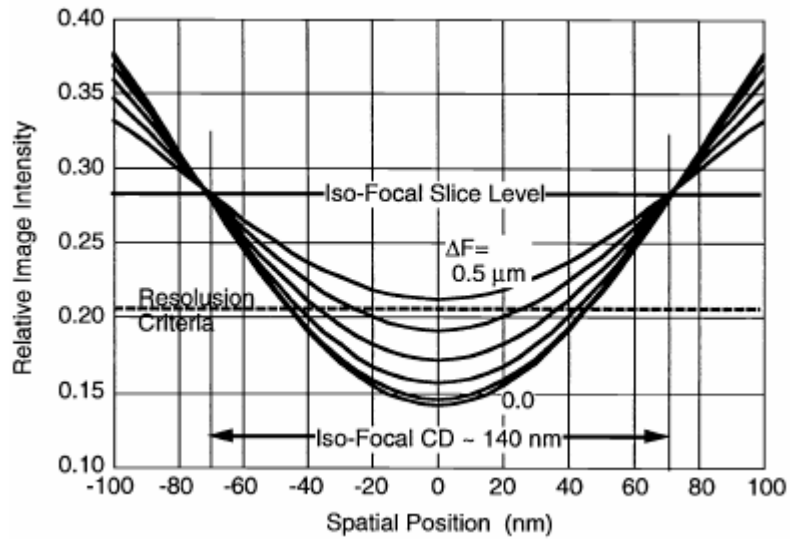
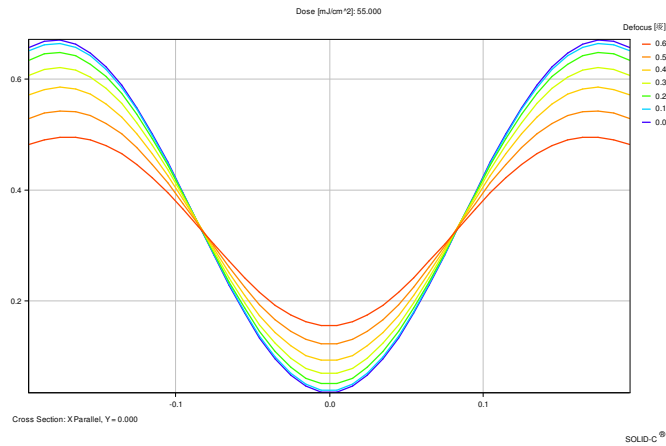
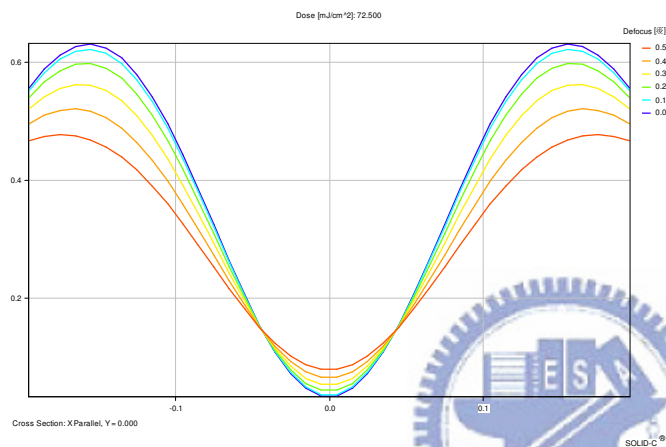


Fig. 4-5 Image intensity profiles of a bright lines pair mask under conditions of CoG mask and conventional illumination. $NA=0.60$, $\sigma=0.85$.



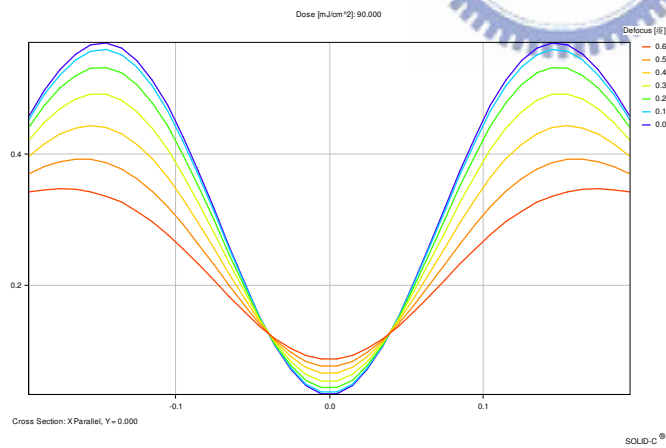
minimum intensity=0.034
iso-focal intensity=0.327

(a) 190nm



minimum intensity=0.034
iso-focal intensity=0.148

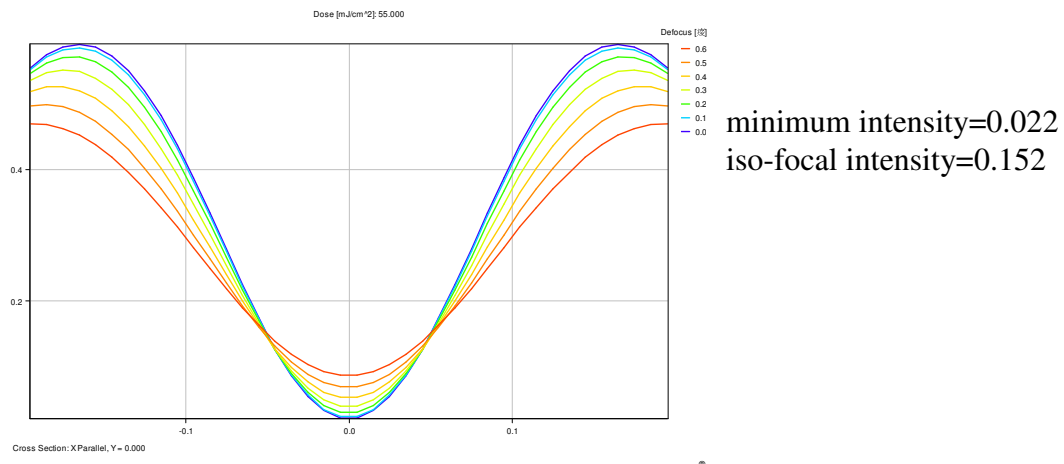
(b) 170nm



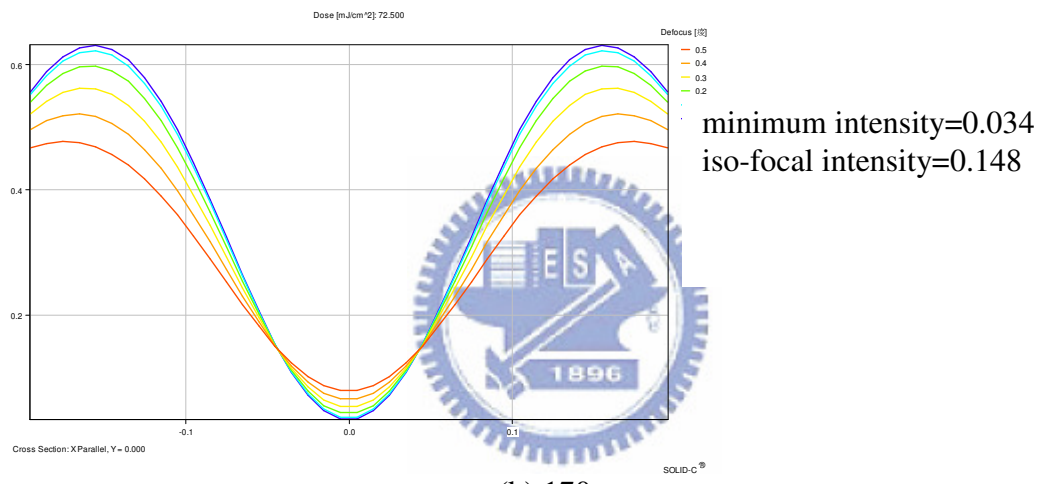
minimum intensity=0.034
iso-focal intensity=0.125

(c) 150nm

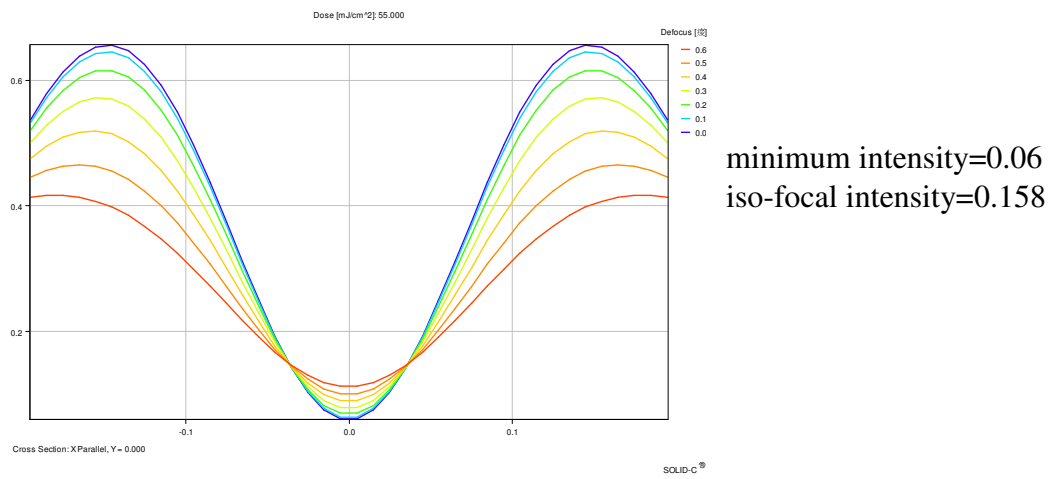
Fig. 4-6 Image intensity profiles with changing bright line width of the bright lines pair for the width of (a)190nm (b) 170nm (c) 150nm



(a) 190nm

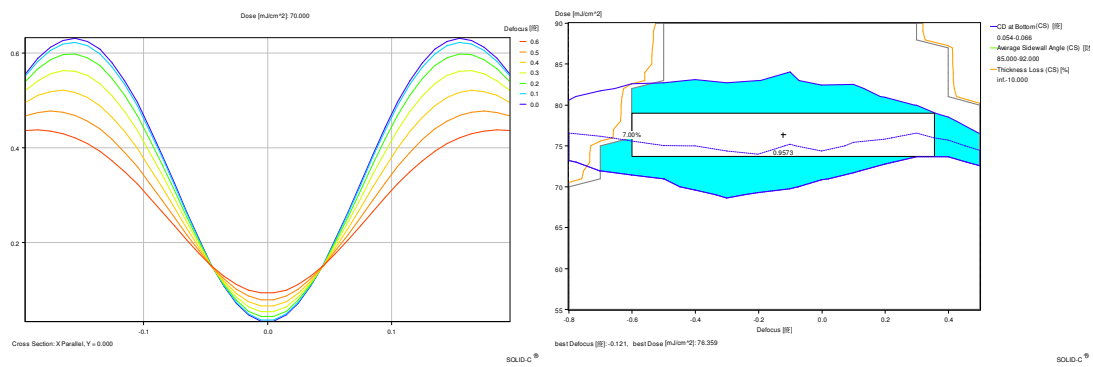


(b) 170nm



(c) 150nm

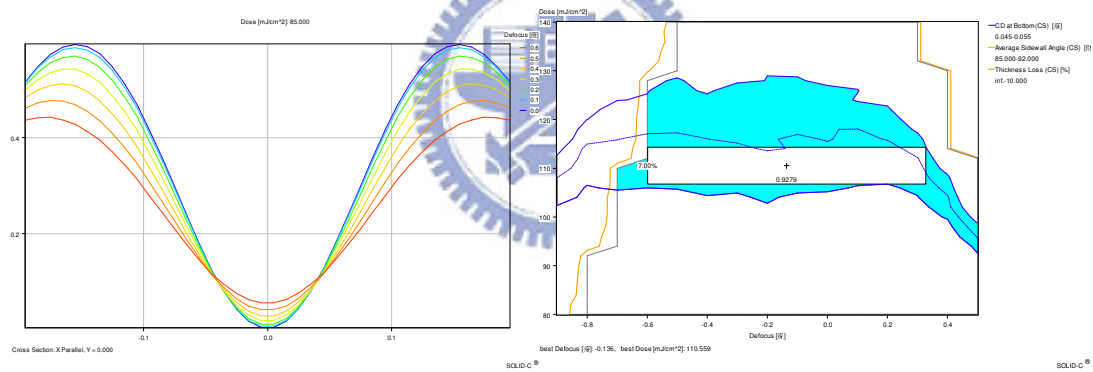
Fig. 4-7 Image intensity profiles with changing dark line width between the bright lines pair (a) 190nm (b) 170nm (c) 150nm



iso-focal intensity=0.15
 minimum intensity=0.034

width=60nm
 DOF=0.9573µm

(a)



iso-focal intensity=0.106
 minimum intensity=0.004

width=50nm
 DOF=0.9279µm

(b)

Fig. 4-8 Image intensity profiles and process window for (a) with binary mask (b) with 6% atten-PSM

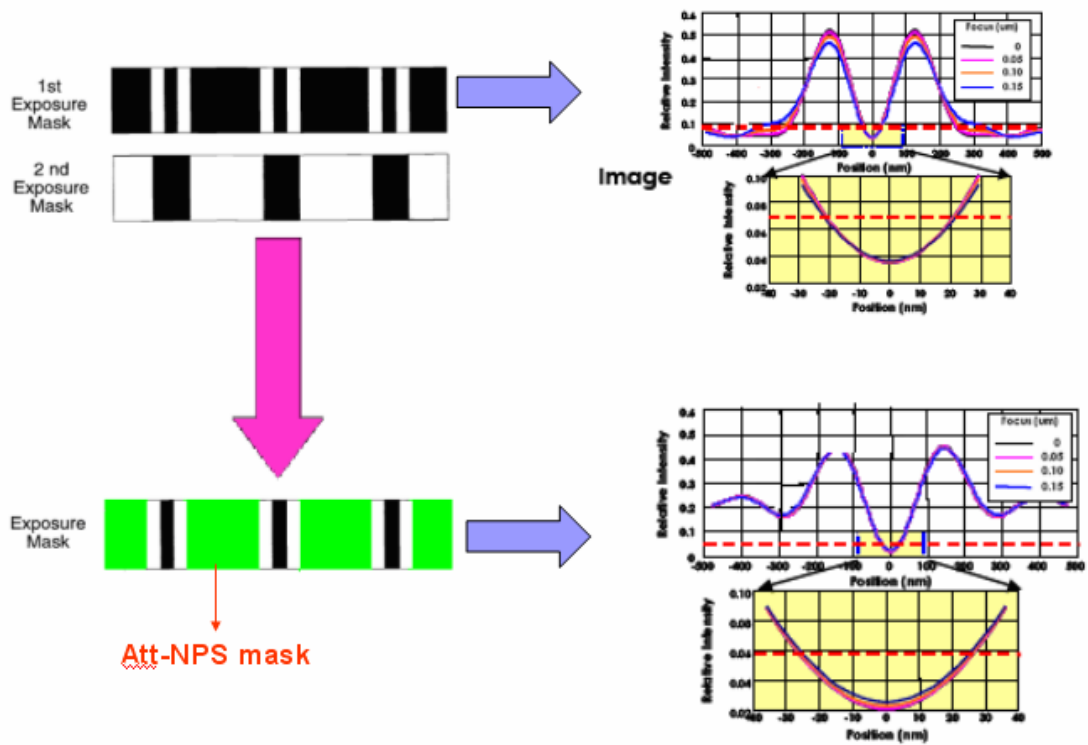


Fig. 4-9 Typical mask patterns and images formed by the mask patterns. (upper) and (lower) show those of the former work and the advanced one, respectively.

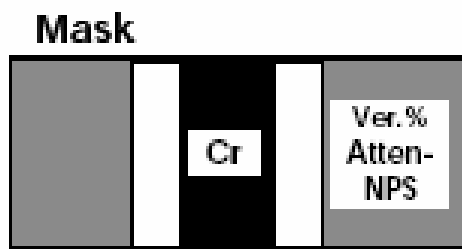


Fig. 4-10 mask of isolated line with changing the transmission of Atten-NPS area

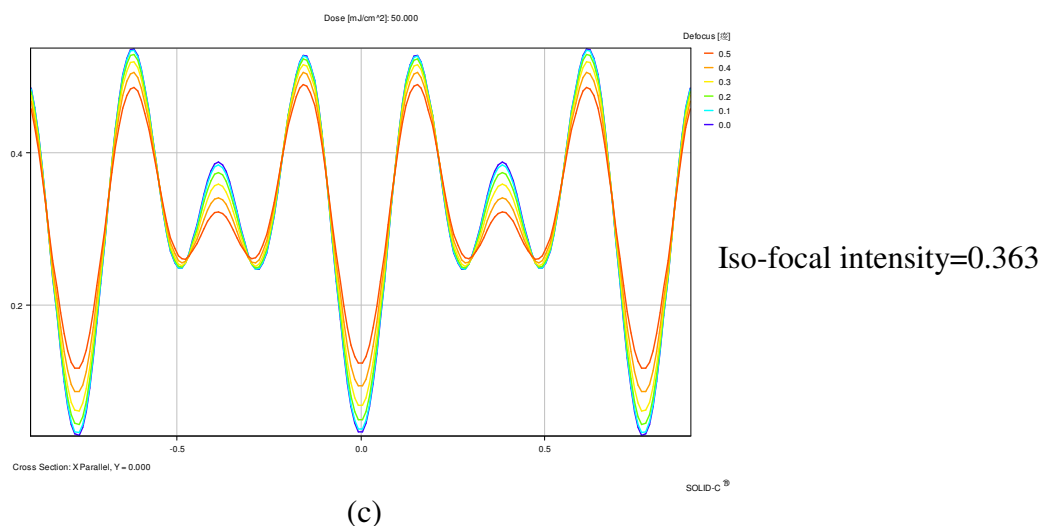
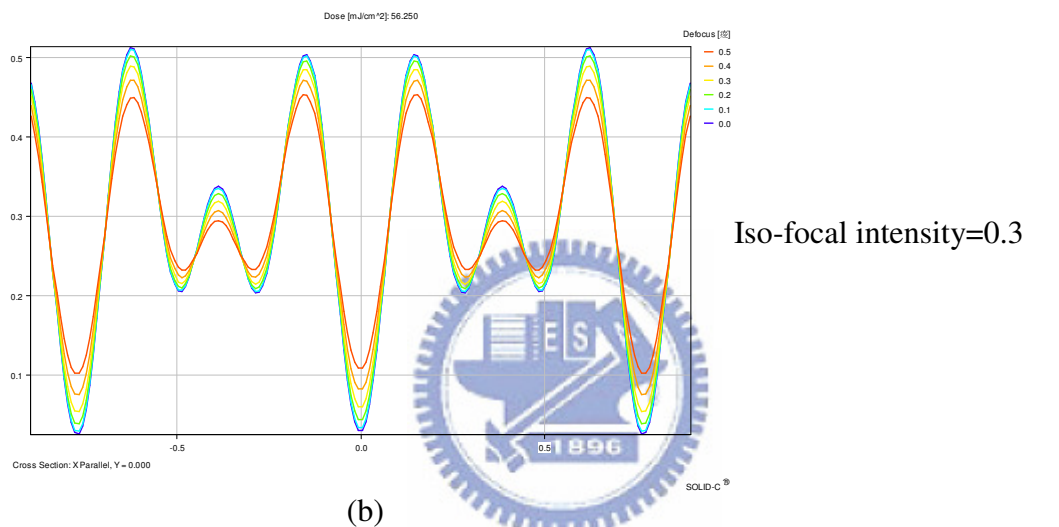
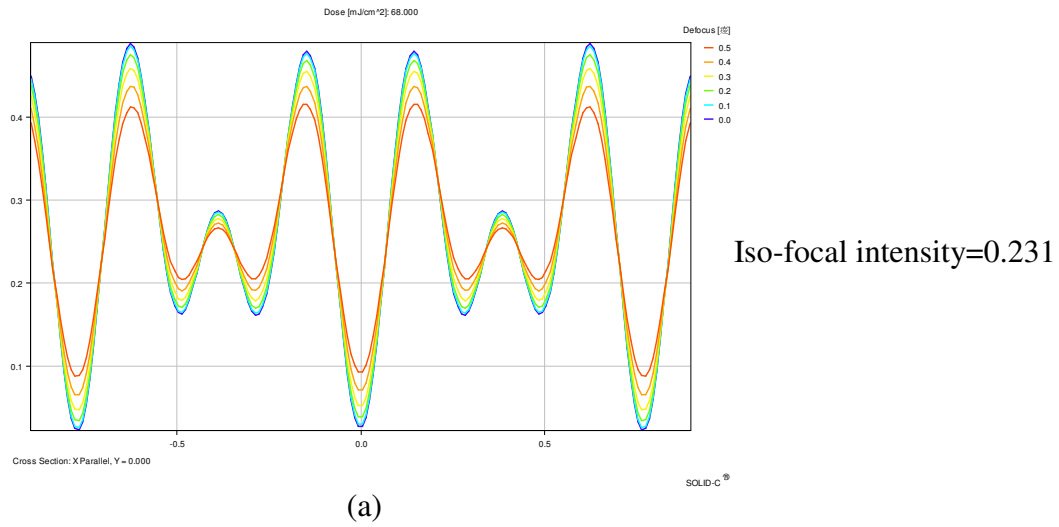
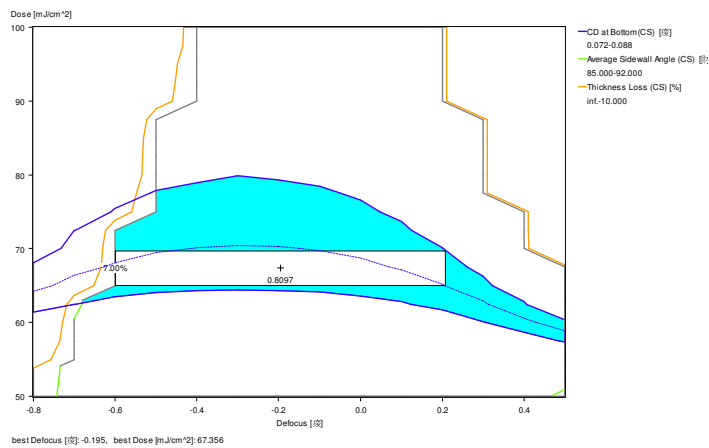


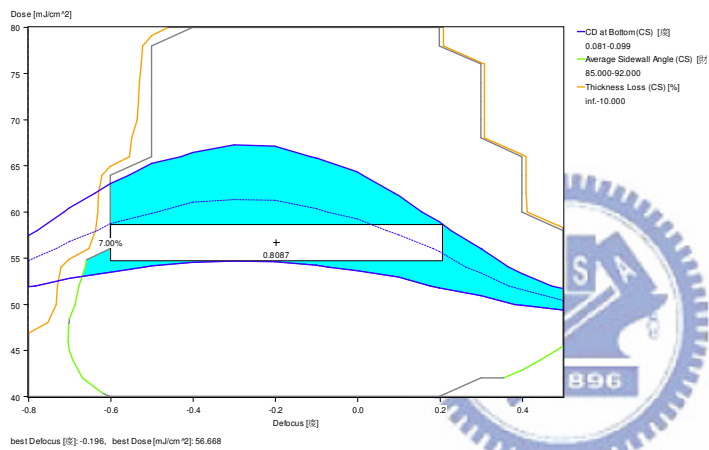
Fig 4-11 aerial image for (a) atten-NPS=20% (b) atten-NPS=25% (c) atten-NPS=30% (dark line=170nm, bright line=90nm, pitch=770nm)



image=80nm
 DOF=0.8097 μ m
 best Dose=67.356

(a)

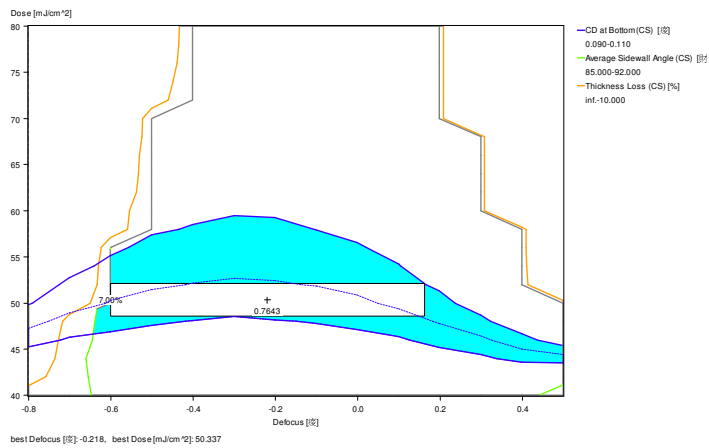
SOLID-C[®]



image=90nm
 DOF=0.8087 μ m
 best Dose=56.668

(b)

SOLID-C[®]



image=100nm
 DOF=0.7643 μ m
 best Dose=50.337

(c)

SOLID-C[®]

Fig 4-12 process window for (a) atten-NPS=20% (b) atten-NPS=25% (c) atten-NPS=30%(dark line=170nm, bright line=90nm, pitch=770nm)

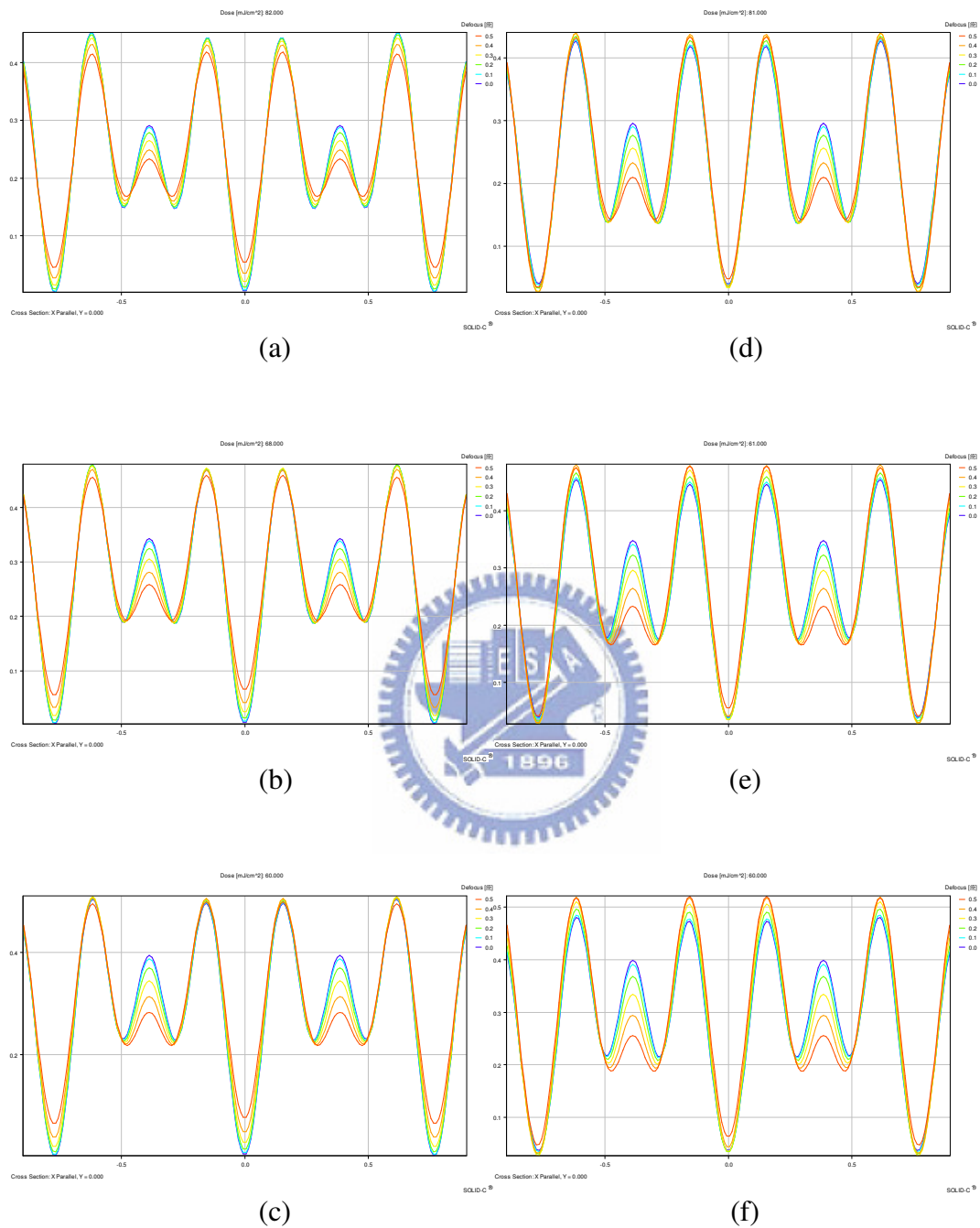
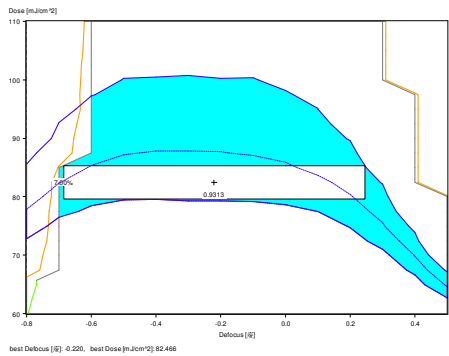
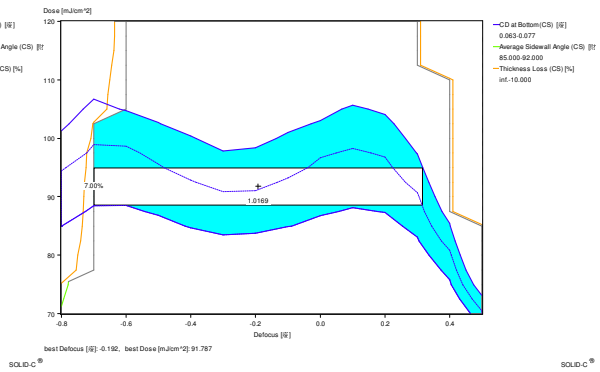


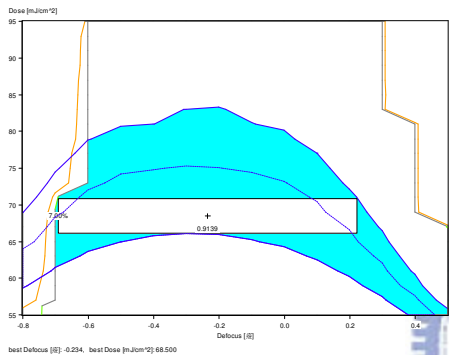
Fig 4-13 aerial image for (a) atten-PSM=6%, atten-NPS=20% (b) atten-PSM=6%, atten-NPS=25% (c) atten-PSM=6%, atten-NPS=30% (d) atten-PSM=20%, atten-NPS=20% (e) atten-PSM=20%, atten-NPS=25% (f) atten-PSM=20%, atten-NPS=30% (dark line=170nm, bright line=90nm, pitch=770nm)



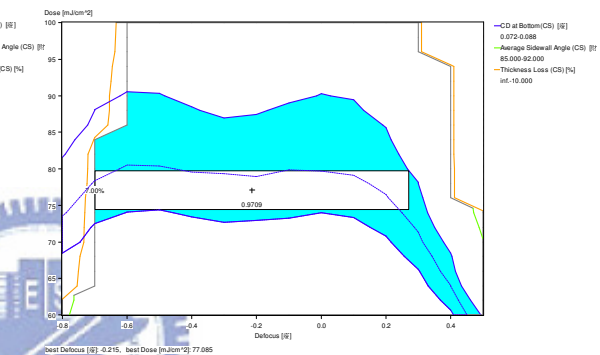
image=80nm DOF=0.9313μm
best Dose=82.466
(a)



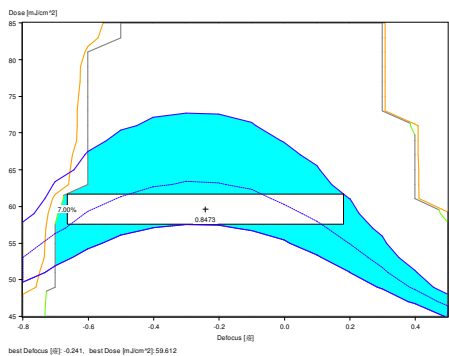
image=70nm DOF=1.0169μm
best Dose=91.787
(d)



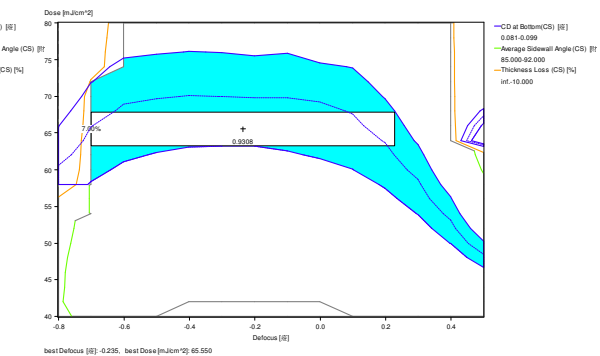
image=90nm DOF=0.9139μm
best Dose=68.5
(b)



image=80nm DOF=0.9709μm
best Dose=77.085
(e)

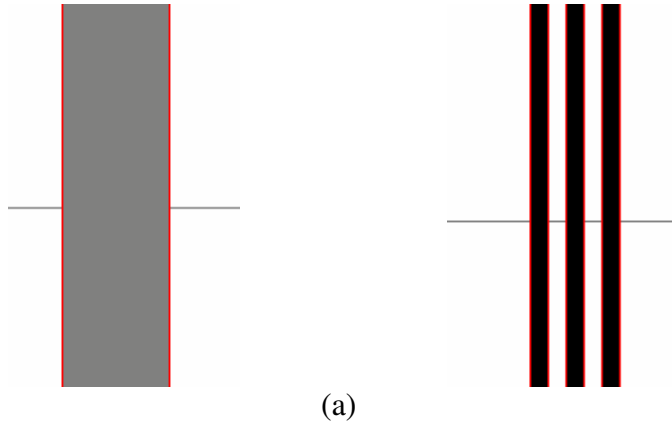


image=100nm DOF=0.8473μm
best Dose=59.612
(c)

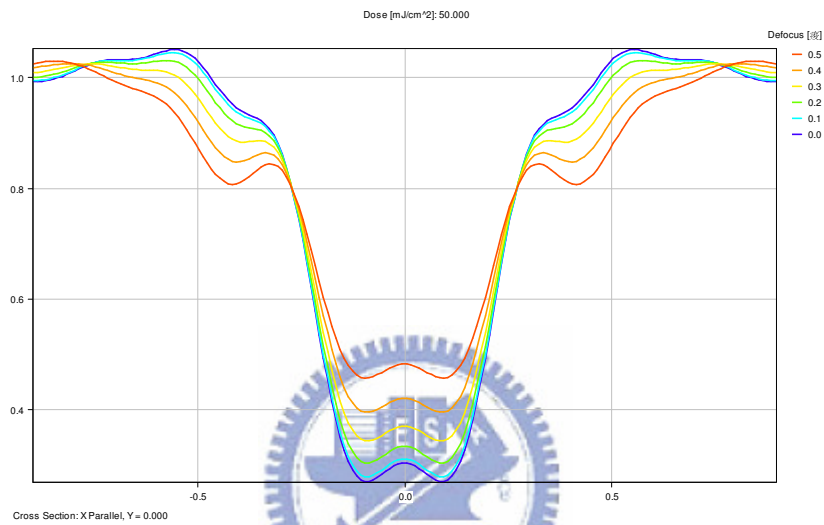


image=90nm DOF=0.9308μm
best Dose=65.550
(f)

Fig 4-14 process window for (a) atten-PSM=6%, atten-NPS=20% (b) atten-PSM=6%, atten-NPS=25% (c) atten-PSM=6%, atten-NPS=30% (d) atten-PSM=20%, atten-NPS=20% (e) atten-PSM=20%, atten-NPS=25% (f) atten-PSM=20%, atten-NPS=30% (dark line=170nm, bright line=90nm, pitch=770nm)

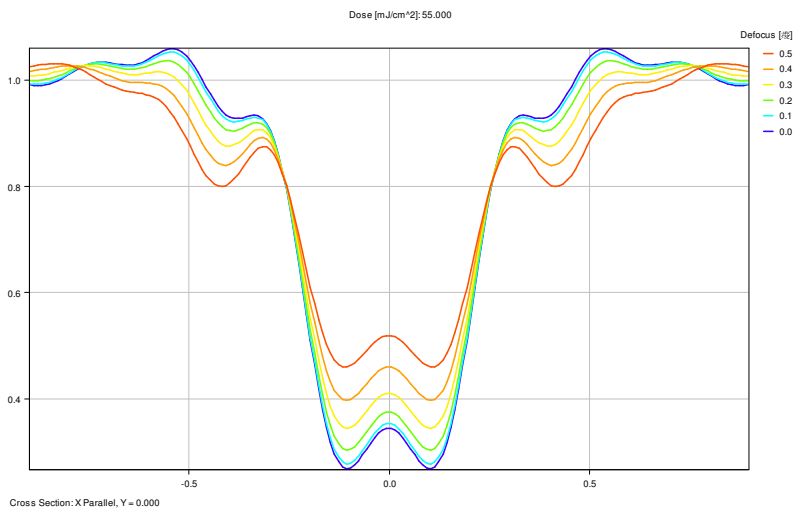


(a)



Minimum intensity=0.268

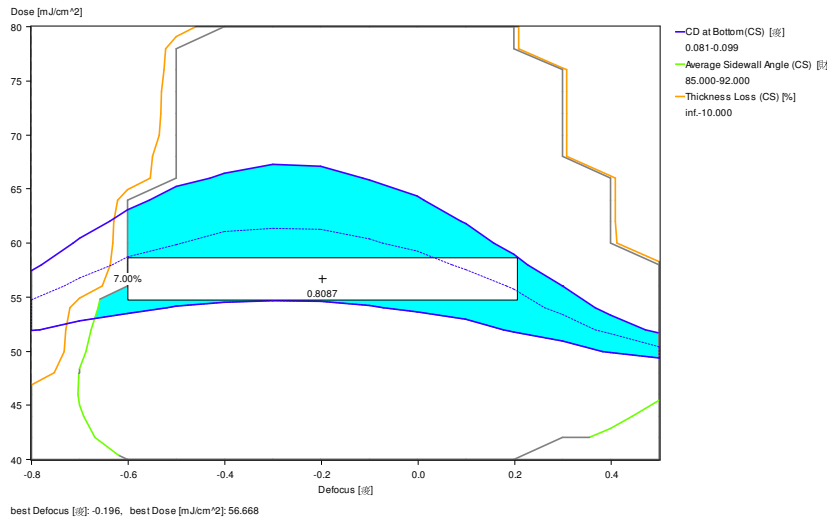
(b)



Minimum intensity=0.266

(c)

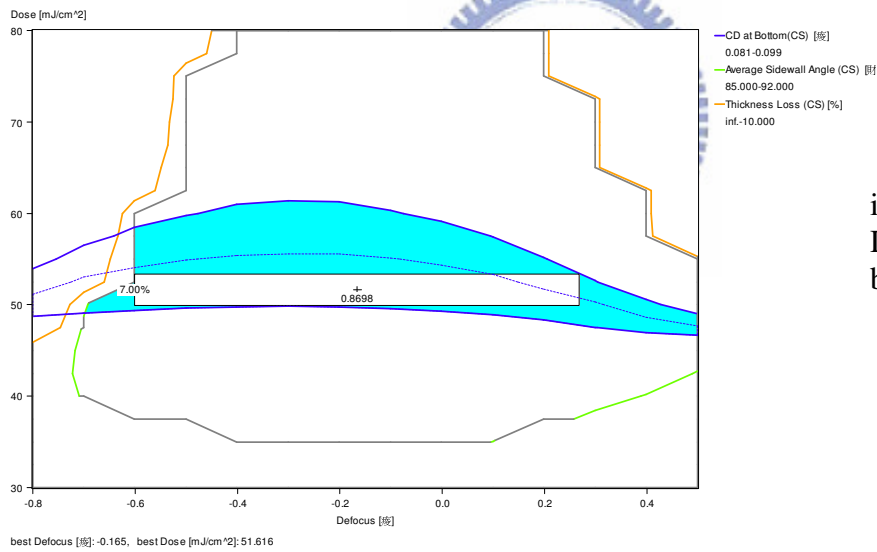
Fig.4-15 (a) mask (b) aerial image of Atten-NPS=0.25 (width=420nm) (c) aerial image of dark line width=68nm and pitch=140nm



image=90nm
DOF=0.8087μm
best Dose=56.668

SOLID-C®

(a)



image=90nm
DOF=0.8698μm
best Dose=51.616

SOLID-C®

(b)

Fig 4-17 process window for (a) Atten-NPS =25% (b) equal binary mask (dark line=67nm, pitch=140nm)

Chapter 5

Conclusion

5-1 Conclusion

It is found that the dark line between a bright lines pair can decrease the iso-focal intensity so to gain a better line pattern. But because in the pair bright lines mask undesirable dark line is formed between adjacent pairs, so it needs double exposure to erase the undesirable dark line.

In order to decrease the time of exposure step, so we change the dark lines between the pair of bright lines with non-phase shifting mask to increase the aerial image intensity of the place. So the original aerial image intensity which is low and can not be resolved will become high enough and can resolve.

Finally, we change the non-phase-shifting mask to a set of line patterns. The line patterns have small width that is below the resolution limit so will not be resolved and the patterns have the similar transmission behavior as non-phase-shifting mask so can be the replaced mask of non-phase-shifting mask.

The schemes of the three methods are shown in figure 5-1. And the simulated results are shown in figure 5-2. From the simulation results can improve our conclusion of above.

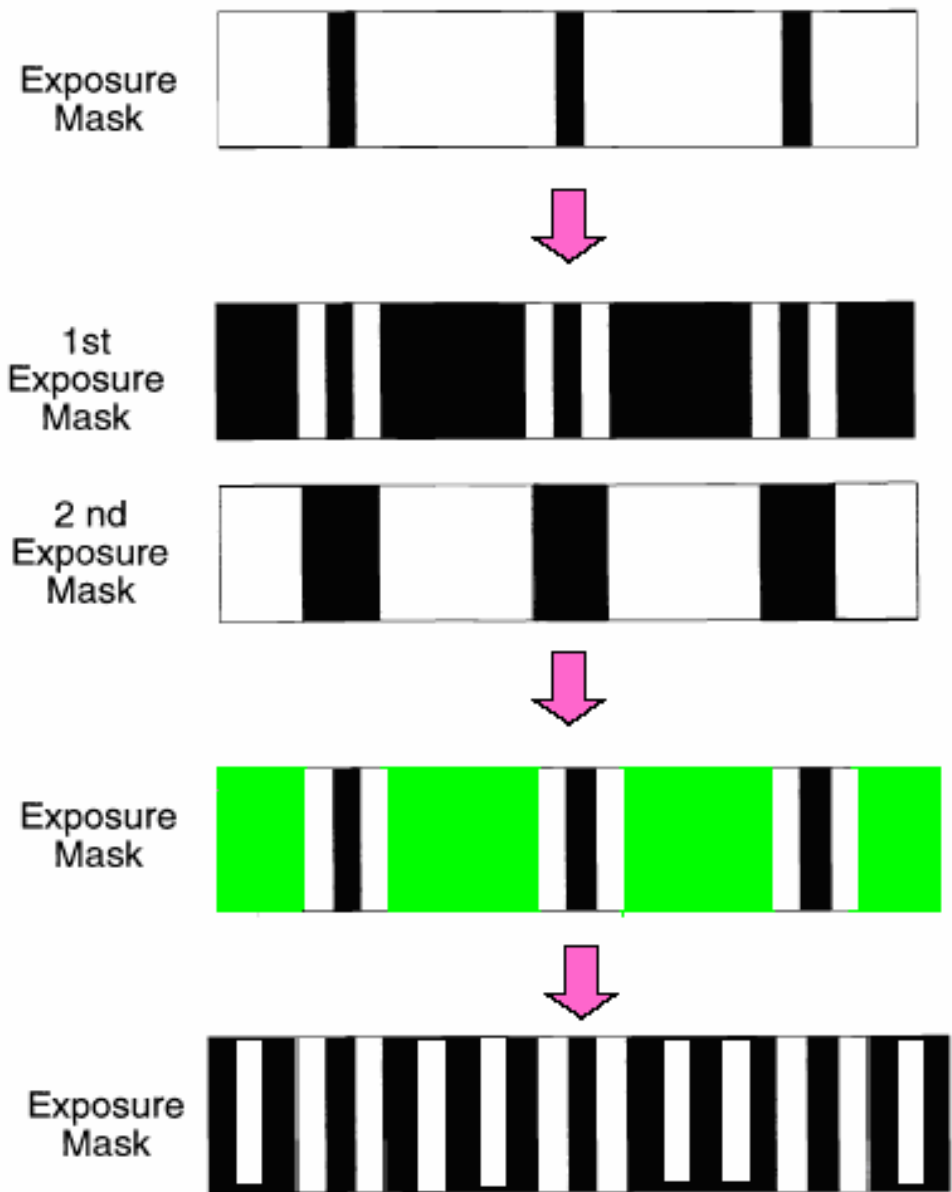
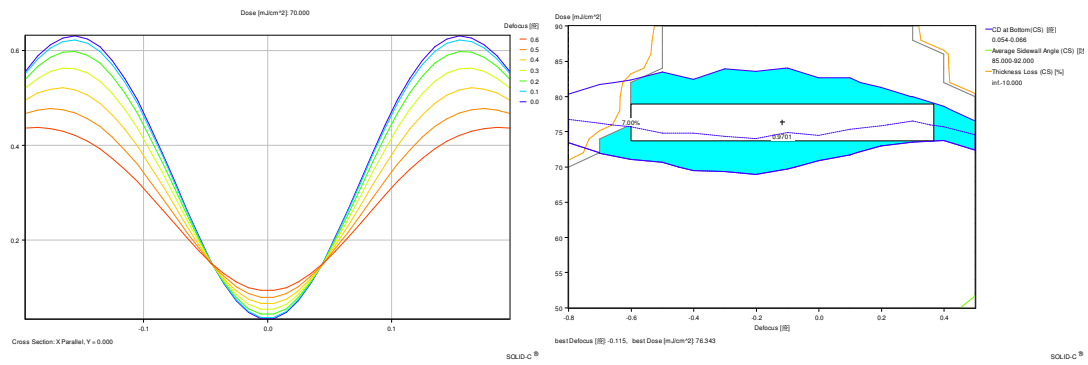
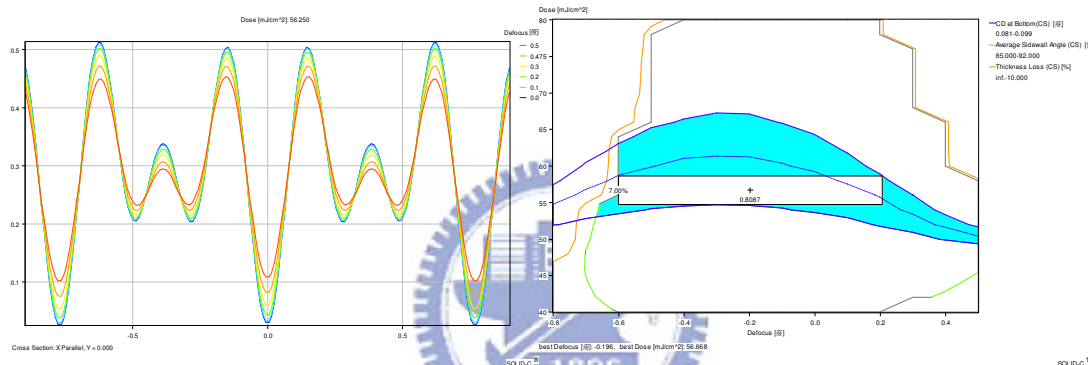


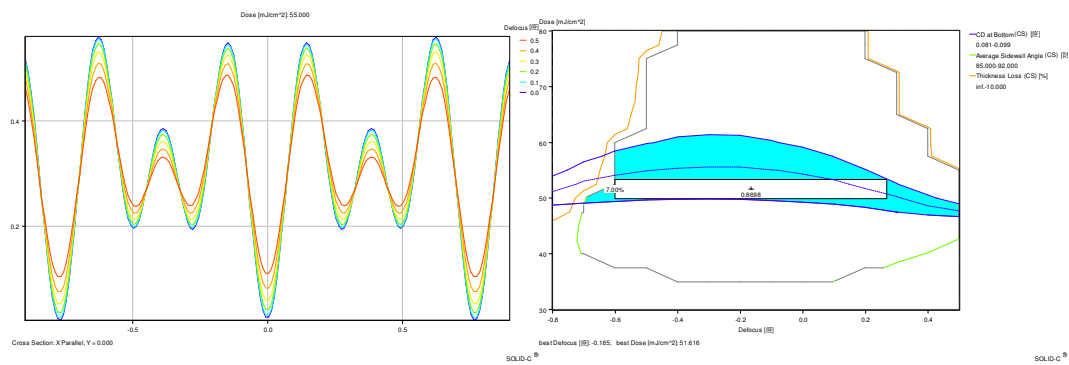
Fig 5-1 scheme of the three methods



width=60nm
 DOF=0.9701 μm
 (a) double exposure



image=90nm
 DOF=0.8087 μm
 (b) Att-NPS



image=90nm
 DOF=0.8698 μm
 (c) binary line equal to Att-NPS

Fig 5-2 process window and aerial image for three methods

Reference

- [1] Semiconductor Industry Association, International Technology Roadmap for Semiconductors: 1999. Austin, TX: SEMATECH, 1999.
- [2] Tsuneo Terasawa, "Subwavelength Lithography (PSM,OPC)", IEEE, pp.295-300, 2000
- [3] H. Fukuda, A. Imai, T. Terasawa, and S. Okazaki, "New Approach to Resolution Limit and advanced Image Formation Techniques in Optical Lithography", IEEE. Trans. Electron Devices, Vol. ED-38, No. 1, pp.67-15, 1991.
- [4] R. Bunaw and H. Fukuda, "Printing Isolated Feature with $kl=0.2$ Using Multi-Plane Exposure", Jpn. J. Appl. Phys., Vol. 35, No. 12B, pp. 6400-6403, 1996.
- [5] J. Finders, A.M. Mulders, J. Krist, D. Flagello, P. Luehrmann, et al., "Sub-0.25 micron lithography applying illumination pupil filtering (quadrupole) on a DUV step & repeat system."
- [6] H. Fukuda, A. Imai, and S. Okazaki, "Phase-Shifting mask and FLEX method for Advanced Photolithography", Proc. SPIE, Vol. 1264, pp. 14-25, 1990.
- [7] HIROSHI FUKUDA, NORIO HASEGAWA, et, "A New Method for Enhancing Focus Latitude in Optical Lithography: FLEX", IEEE ELECTRON DEVICE LETTERS, VOL. EDL-8, NO. 4, APRIL 1987
- [8] Hiroshi Fukuda, Tsuneo Terasawa, and Shinji Okazaki, "Spatial filtering for depth of focus and resolution enhancement in optical lithography", American Vacuum Society, pp. 3113-3116, 1991
- [9] M. Noguchi, M. Muraki, Y. Iwasaki, and A. Suzuki, "Subhalf Micron Lithography System with Phase Shifting Effect", Proc. SPIE symp. Microlithography, Vol. 1674, pp. 92-104, Mar. 1992.
- [10] K. Kamon, T. Miyamoto, Y. Myoi, H. Nagata, M. Tanaka, and K. Horie, "Photolithography system using annular illumination," Jpn. J. Appl. Phys., pt. 1, vol. 30, p. 3012, 1991.
- [11] B.J. Lin, Linnovation, Inc. Off-axis illumination -- Working principles and comparison with alternating phase-shifting masks SPIE Vol. 1927 Optical/Laser Microlithography VI (1993) / 89
- [12] Jan van Schoot, Jo Finders, Koen van Ingen Schenau, Michel Klaassen and

Corine Buijk “THE MASK ERROR FACTOR: CAUSES AND IMPLICATIONS FOR PROCESS LATITUDE” SPIE Vol. 3679 p250

- [13] B.J. Lin, Linnovation, “Off-axis illumination -- Working principles and comparison with alternating phase-shifting masks”, SPIE, Vol. 1927, pp.89-100, 1993
- [14] M. D. Levenson, N. S. Viswanathan, and R. A. Sympson, “Improving Resolution in photolithography with a Phase-Shifting Mask”, IEEE, Trans. Electron Devices, Vol. ED-29, No. 12, pp. 1828- 1836, 1982.
- [15] T. Terasawa, N. Hasegawa, T. Tanaka, S. Katagiri, and T. Kurosaki, “Improved resolution of an i-line stepper using a phase-shifting mask”, J. Vuc. Sci. Techno!., Vol. B8, No.6, pp. 1300-1308, Nov/Dec. 1990.
- [16] A. Nitayama, T. Sato, K. Hashimoto, E Shigematsu, and M Nakase, “New Phase Shifting Mask with Self-aligned Phase Shifter for Quarter Micron Photolithography”, Technicul Dig., pp.57-60, Dec. 1989.
- [17] T. Terasawa, N. Hasegawa, H. Fukuda, and S. Katagiri, “Imaging characteristics of Multi-Phase-Shifting and Halftone phase Shifting Masks”, Jpn.J. Appl. Phys., Vol. 30, No. 11, pp. 2991-2997, 1991.
- [18] H.-Y. Liu, L. Karklin, Y.-T. Wang, and Y.C. Pati, “The application of phase-shifting masks to 140 nm gate patterning (II): Mask tolerances,” Proc. SPIE, vol. 3334, p. 2, 1998.
- [19] H.-Y. Liu, L. Karklin, Y.-T. Wang, and Y. C. Pati, “The application of alternating phase-shifting masks to 140 nm gate patterning: Line width control improvements and design optimization,” in Proc. SPIE, vol. 3236.,1997
- [20] B. J. Lin, “The attenuated phase-shifting mask,” Solid State Technol., vol. 35, pp. 43–47, January 1992.
- [21] B.J. Lin, “Phase-Shift ing Masks Gain an Edge”, Circuits & Devices, pp.28-35, 1993
- [22] K. Toh, G. Dao, R. Singh, and H. Gaw, “Chromeless phase-shifted masks: A new approach to phase-shifting masks,” in Proc. SPIE, vol. 1496, pp. 27–53, 1990
- [23] J. F. Chen, J. Petersen, R Socha, T Laidig, K. Wampler, K. Nakagawa, G. Hughes, S. MacDonald, and W. Ng, “Binary halftone chromeless PSM technology for $\lambda/4$ optical lithography”, Proc. SPIE 4346, pp.515-533 , 2001.
- [24] C. Hsu, R. Chu, J. F. Chen, D. J. Van Den Broeke, X. Shi, S. D. Hsu, and T. Wang, “Patterning half-wavelength DRAM cell using Chromeless Phase Lithography

- (CPL)", Proc. SPIE 4691, pp.76-88, 2002
- [25] Jan van Schoot, Jo Finders, Koen van Ingen Schenau, Michel Klaassen and Corine Buijk, "THE MASK ERROR FACTOR: CAUSES AND IMPLICATIONS FOR PROCESS LATITUDE", SPIE , Vol. 3679, pp.250-260, 1999
- [26] Richard Rogoff, Guy Davies, Jan Mulkens, Jos de Kierk, Peter van Oorschot, "PHOTOLITHOGRAPHY USING THE AERIALTM ILLUMINATOR IN A VARIABLE NA WAFER STEPPER", SPIE, Vol. 2726, pp.54-70,
- [27] Nakao, K. Narimatsu, T. Miyagi, S. Ogawa, N. Tamada, A. Nakae, A. Tokui, K. Tsujita, I. Arimoto, W. Wakamiya, "Innovative Imaging of Ultra-fine Line without Using Any Strong RET", Proc. SPIE, 4346, 503 (2001).
- [28] M. Born and E. Wolf, Principles of Optics, 6th ed.
- [29] J. A. Torres, "Contrast analysis and optimization for resolution enhancement technique" 2003 Society of Photo-Optical Instrumentation Engineers
- [30] M. Sanchez, W. Hinsberg, F. Houle, J. Hoffnagle, H. Ito, and C. Nguyen, "Aerial image contrast using interferometric lithography: Effect on line-edge roughness," in Proc. SPIE, W. Conley, Ed., 1999, vol. 3678, pp. 160–171.
- [31] J. Shin, G. Han, Y. Ma, K. Moloni, F. Cerrina, "Resist Line Edge Roughness and Aerial Image Contrast", J. Vac. Sci. Technol. B, 19(6), 2890 (2001).
- [32] B. G. Kim, S. W. Choi, W. S. Han, and J. M. Sohn, "Beneath the MEEF," Solid State Technol., vol. 43, no. 8, p. 107, 2000.
- [33] Chun-Kung Chen, Tsai-Sheng Gau, Jaw-Jung Shin, Ru-Gun Liu, Shinn-Sheng Yu, Anthony Yen and Burn J. Lin, "Mask Error Tensor can Causality of Mask Error Enhancement for Low-k₁ Imaging: Theory and Experiments", TSMC corporation
- [34] J. van Schoot, J. Finders, and C. Buijk, "The mask error factor: Causes and implications for process latitude," Proc. SPIE, vol. 3679, pp. 250–260.
- [35] Chris A. Mack, "Resolution and Depth of Focus in Optical Lithography", SPIE, Vol.3183, pp.14-27
- [36] D. Fuard, P. Schiavone and M. Besacier " Validity of the diffused aerial image model: an assessment based on multiple test cases", Proc of SPIE, vol.5040 p.1536, (2003)
- [37] J. Van Wingerden et al. " Lithographic process optimisation using process capability analysis", Proc of SPIE, vol.5040 p.882-893, (2003)
- [38] T. Terasawa, N. Hasegawa, "Theoretical Calculation of Mask Error Enhancement Factor for Periodic Pattern Imaging", Jpn. J. Appl. Phys., 39, 6786 (2000).

個人簡歷

姓名：曹人傑

性別：男

出生年月日：民國 72 年 4 月 6 日

住址：彰化市桃源里虎崗路五號

學歷：

國立彰化師範大學機電工程系學士 (91.9-94.6)

國立交通大學電子研究所碩士 (94.9-96.7)

碩士論文題目：

使用一次曝光和二元光罩來產生擁有良好聚焦深度的細線之模擬與
研究

The Study and Simulation of the Line Pattern having large Depth of
Focus by using only Single Exposure and Binary Mask